



# Synoptic timescale linkage between midlatitude winter troughs Sahara temperature patterns and northern Congo rainfall: A building block of regional climate variability

Neil Ward<sup>1</sup>  | Andreas H. Fink<sup>2</sup>  | Richard J. Keane<sup>1,3</sup> |  
 Françoise Guichard<sup>4</sup> | John H. Marsham<sup>1,5</sup> | Douglas J. Parker<sup>1</sup> |  
 Christopher M. Taylor<sup>6,7</sup>

<sup>1</sup>School of Earth and Environment,  
University of Leeds, Leeds, UK

<sup>2</sup>Institute for Meteorology and Climate  
Research, Karlsruhe Institute for  
Technology, Karlsruhe, Germany

<sup>3</sup>Met Office, Exeter, UK

<sup>4</sup>Centre National de Recherches  
Météorologique (CNRM), UMR 3589,  
Centre de la Recherche Scientifique  
(CNRS) Météo-France and Université de  
Toulouse, Toulouse Cedex, France

<sup>5</sup>National Centre for Atmospheric Science  
(NCAS), Leeds, UK

<sup>6</sup>UK Centre for Ecology and Hydrology,  
Wallingford, UK

<sup>7</sup>National Centre for Earth Observation,  
Wallingford, UK

## Correspondence

Neil Ward, School of Earth and  
Environment, University of Leeds,  
Leeds, UK.

Email: wardn626@gmail.com

## Funding information

German Research Foundation;  
Transregional Collaborative Research  
Center 165 "Waves to Weather"; Global  
Challenges Research Fund, African  
SWIFT programme, Grant/Award  
Number: NE/P021077/1; IMPALA, Grant/  
Award Number: NE/M017230/1; AMMA-  
2050, Grant/Award Numbers: NE/  
M020428/2, NE/M019950/1,  
NE/M017176/1, NE/M020126/1

## Abstract

A coherent synoptic sequence, mostly over North Africa, is identified whereby an upper-level midlatitude trough (in November–March) excites several days of quasi-stationary near-surface warming across the Sahara, leading to rainfall events over northern Congo (NC), and perturbed weather more widely. Ahead of NC rainfall events, composite sequences first identify troughs for several days near Iberia, followed by relatively quick transfer to the Central Mediterranean (CMed). Iberia and CMed daily trough-strength indices reveal that both lead to warming and NC rainfall. Iberia trough linkages develop through West Africa and take longer to reach NC, while CMed linkages reach NC faster (2–3 days), with impact extent focused mostly south and east of CMed. Building up to the rainfall events, initial warming over the central Sahara migrates southeastward close to NC, ultimately with typical magnitude of about 1–2°C at 10–15°N. Such anomalies are statistically predictive for NC daily rainfall and associated nearby atmospheric features: anomalous low-level southerly wind and increased moisture; anomalous low-level westerly wind and vertical easterly shear to 600 hPa; increased mid-level moisture (600 hPa), which along with low-level moisture, connects northward into midlatitudes. A secondary route identified by which Iberia troughs can impact NC rainfall is through direct atmospheric teleconnection with precipitation to the west of NC, and subsequent migration of that convection eastward into NC. The eastern side of NC generally shows a small lag on western parts, and links more strongly to CMed troughs. Taken together, the lagged synoptic expression of Iberia and CMed troughs is widespread over several days, including much of North Africa (to equatorial latitudes), southwestern Asia, eastern Africa and the western Indian Ocean. Overall, these results can contribute to situational awareness for weather forecasters across the zones influenced by the troughs, while also providing a framework for climate timescale analyses.

This is an open access article under the terms of the Creative Commons Attribution-NonCommercial License, which permits use, distribution and reproduction in any medium, provided the original work is properly cited and is not used for commercial purposes.

© 2021 The Authors. *International Journal of Climatology* published by John Wiley & Sons Ltd on behalf of the Royal Meteorological Society.

**KEYWORDS**

climate teleconnections, Congo rainfall, midlatitude troughs, North Africa, Rossby waves, Sahara temperature, synoptic weather

**1 | INTRODUCTION**

Boreal winter months represent a minimum of precipitation in the annual cycle of the northern part of the Congo Basin (hereafter NC). Substantial rain does still occur (November–March contributes about 20–25% of the annual total), but it is normally considered the dry season, with the bulk of the Congo rainfall belt lying to the south in these months. Research has mostly focused on the main rainy seasons in the Congo region, with interannual and longer timescale rainfall fluctuations attributed to variations in tropical sea-surface temperatures, the Walker circulations, and associated changes in the atmospheric moisture budget over the Congo Basin (Hirst and Hastenrath, 1983; Camberlin *et al.*, 2001; Todd and Washington, 2004; Balas *et al.*, 2007; Samba and Nganga, 2012; Dezfuli and Nicholson, 2013; Nicholson and Dezfuli, 2013; Washington *et al.*, 2013; Hua *et al.*, 2018).

However, recently, Taylor *et al.* (2018; hereafter T18) uncovered very different teleconnection structures associated with NC in February, revealing linkages between NC mesoscale convection systems (MCSs) and monthly-mean anomalous conditions northward across the Sahara and into northern midlatitudes. At the synoptic timescale, several days of low-level warming across northeastern Africa (hereafter NE Africa, more precisely, over the eastern Sahara and Sahel) tended to precede the most intense MCSs over the eastern part of NC (hereafter, NEC), with apparent connection to midlatitude upper-level troughs to the north. The purpose of this study is to establish the extent to which the daily sequence in T18 is a systematic feature of boreal winter weather and climate across North Africa, and to better isolate the role of midlatitude troughs.

Very few studies have attempted to establish midlatitude linkages to Congo rainfall. In one example, using a broad Congo Basin index, Todd and Washington (2004) did find connection to the North Atlantic Oscillation (NAO); however, the focus on NC indices in T18 reveals very different structures. Some other boreal winter midlatitude linkages to North Africa do prove useful in framing the NC connections. These include linkages to West Africa (Knippertz and Fink, 2008), Ethiopia (Camberlin and Philippon, 2002; Bekele-Biratu *et al.*, 2018), and eastern Sahara cold surges (Vizy and Cook, 2014).

Improved understanding of this problem has broader relevance given anticipated climate variability linkages into both hemispheres. In addition, NC rains at this time of year, while weaker, are still societally important, for

example, impacting agricultural practices including burning, planting, and harvesting (Wilkie *et al.*, 1999; Salerno *et al.*, 2019). The synoptic linkages in T18 and expanded upon here have the potential to lead to improvements in weather forecasting over NC and North Africa generally (e.g., Davis *et al.*, 2013), especially given the low levels of skill in raw and postprocessed ensemble rainfall predictions in many parts of the impacted region (Vogel *et al.*, 2020). A role for the synoptic linkages in climate variations across different timescales is also anticipated (e.g., Skinner and Poulsen, 2016).

Data, methods and overview of NC climate are presented in Section 2. The article then proceeds (Section 3) by exploring how strong daily rainfall/convection events over NC during November–March display the North Africa and midlatitude signature found in T18. While these analyses are indicative of a role for midlatitude troughs, they do not establish that this linkage is the primary feature of downstream conditions following troughs. Section 4 therefore calculates indices of trough strength and diagnoses the evolution of conditions over several days following the strongest upper-level troughs over the Atlantic/Mediterranean sector. Results suggest that troughs anchored near Iberia and the Central Mediterranean (CMed) may be key for NC (via NE Africa warming), so the detailed expression of these troughs is diagnosed. Next, Section 5 focuses explicitly on the linkage between NE Africa warming and subsequent response over NC, diagnosing nearby atmospheric features in the days before and during active NC days, and expanding analysis to all days through linear correlation and regression. Section 6 considers the relation of monthly teleconnection structures to the several-day synoptic sequence identified. Section 7 provides concluding discussion.

**2 | DATA, METHODS, AND NORTH CONGO CLIMATE CONTEXT****2.1 | Data**

Daily mean reanalysis fields are used from the European Centre for Medium-Range Weather Forecasts (ECMWF) product ERA5 (Hersbach *et al.*, 2020), downloaded at the same resolution ( $0.75^\circ \times 0.75^\circ$ ) as the earlier product ERA-I (Dee *et al.*, 2011). This permitted direct comparisons between ERA5 and ERA-I, building on the results of T18 with ERA-I. The chosen resolution is considered

sufficient to diagnose the relatively large-scale features under analysis; the purpose is not to diagnose the details of precipitation events themselves, instead the broad environment and remote teleconnections in which they develop.

As a proxy for tropical rainfall and convection, the interpolated daily outgoing longwave radiation (OLR) (Liebmann and Smith, 1996) dataset is used. It is based on twice-daily polar orbiting satellite measurements, and provided on a  $2.5^\circ \times 2.5^\circ$  grid. It has been widely used in studies of this kind addressing tropical convection and rainfall (e.g., Laing *et al.*, 2011; Van der Wiel *et al.*, 2015).

Most analyses reported use OLR and ERA5 over 1982–2016. In addition, for further validation, some results are produced over 2001–2016 with the shorter precipitation record from: Multi-satellitE Retrievals for GPM (IMERG V6), which calibrates and merges multiple satellite and ground-based sources into a gridded product (Huffman *et al.*, 2019), here downloaded to daily values for the same grid as the OLR. Earlier versions of similarly-processed data (TMPA 3b42) compared favourably with other products over this relatively data-sparse region of central Africa (Camberlin *et al.*, 2019).

## 2.2 | Methods

For each variable analysed, a background daily climatology (for 1982–2016, except for IMERG, 2001–2016) has

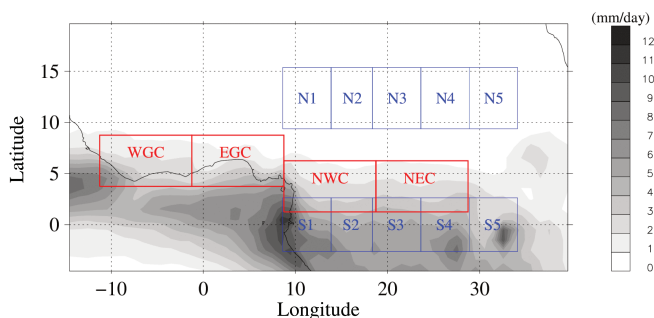


**FIGURE 1** November–March precipitation (IMERG) climatology (2001–2016) and selected index domains. Red: Northeast Congo (NEC), Northwest Congo (NWC), East Guinea Coast (EGC), and West Guinea Coast (WGC), used for OLR, precipitation, and various reanalysis variables; for reference, NEC boundaries shown are  $1.25\text{--}6.25^\circ\text{N}$ ,  $18.75\text{--}28.75^\circ\text{E}$ . Blue: low-level temperature indices, with band N1–N5 covering ERA5 grid-boxes centred  $9.75\text{--}15^\circ\text{N}$  (indices referred to as approximately  $10\text{--}15^\circ\text{N}$  in the text). For analyses here, two adjacent boxes are averaged into one index, so N34 measures temperature to the north of NEC and N34 minus S34 measures the broad-scale Sahel-to-Equator temperature gradient operating over the longitudes of NEC [Colour figure can be viewed at [wileyonlinelibrary.com](http://wileyonlinelibrary.com)]

been constructed. After experimentation, the climatology used for day  $i$  is a 31-day climatology centred on day  $i$ , and is used to construct daily anomaly datasets. A number of area-average indices are used for different variables (for reference, most domains used are shown on Figure 1): indices to identify the wettest days in Section 3 use actual values (following T18), but all other indices average the daily anomalies.

Previous studies have defined upper-level midlatitude trough parameter (TP) indices that can be used to explore co-varying features (e.g., Jacobeit, 1987). Here, building on Knippertz (2004) and noting the scale of troughs that precede warming over NE Africa (T18 and results here), the following index is calculated, with averages over  $35\text{--}45^\circ\text{N}$ :

$$TP = \left( \frac{Z_1 + Z_3}{2} \right) - Z_2 \quad (1)$$

where  $Z_2$  is the average geopotential height anomaly at 200 hPa ( $Z_{200}$ ) for a  $10^\circ$  longitude zone centred on the target trough longitude, and  $Z_1$  and  $Z_3$  are average  $Z_{200}$  anomalies for the  $12.5^\circ$  zones to the west ( $Z_1$ ) and east ( $Z_3$ ) of  $Z_2$ . Large values of TP indicate the presence of a strong trough; explicitly, it measures the zonal gradient into the target trough longitude (Knippertz, 2004), and may also be considered a finite difference measure of the curvature associated with the trough.

The value of TP has been calculated for each day for a series of six target longitudes (each separated by  $15^\circ$ ) stretching from the western Atlantic to the eastern Mediterranean. As anticipated by results in Section 3, values of TP targeting Iberia ( $Z_2$  centred at  $2.5^\circ\text{W}$ ) and CMed ( $Z_2$  centred at  $12.5^\circ\text{E}$ ) are relevant for NC (and these points anchor the trough longitudes explored for comparison at  $15^\circ$  longitude intervals). Subsequent work may seek to optimize the choice of the longitudes, and sharpness of the results may also be enhanced through use of upper-level potential vorticity (e.g., Fröhlich *et al.*, 2013). However, the approach here proves a sufficient tool to advance knowledge on the targeted trough linkages.

Mean composite analyses (e.g., Section 3) proceed by first identifying the days of largest values in an anchor index over period  $P$ , and calculating for the same days, the mean daily anomaly at each grid-point in the target field. A second sample is formed from all other days over  $P$ , and the difference calculated, with significance estimated using a  $t$ -test, without assumption of equal variance in the two samples (Afifi and Azen, 1979). The  $t$ -test is only approximate, partly due to distribution assumptions, but also because daily samples may not be independent due to serial correlation in the data. Composites for

1982–2016 and 2001–2016 are useful to compare, especially since the latter avoids a tendency for increased convection in some tropical areas after 1999 (e.g., Hart *et al.*, 2019), and in particular in February over NC (T18). However, most anchor indices used do not contain this change (see Figures S1, S2, S3), such that the targeted synoptic features emerge naturally from the analyses without need for detrending and are mostly consistent over sub-periods within 1982–2016. Results are also found consistent over sensible choices of the percentile cut-off to use for the composite. Most results presented use a threshold of 20% (of all days) following T18, though for OLR indices over 1982–2016, the 10% threshold results are presented for sharpness, with still a large sample size (e.g., for a December analysis this gives a sample of 108 strong event days).

Overall, the methodology followed is to use statistical significance as an aid in physical interpretation, rather than an absolute determinant of conclusion. However, for correlation analysis, methodology is well established

to make estimates of adjustment to significance for positive serial correlation, here using the simplest formulation requiring just an estimate at lag 1 (Bartlett, 1935; Bretherton *et al.*, 1999):

$$N_{\text{ef}} = N \left( \frac{1 - r_1 r_2}{1 + r_1 r_2} \right) \quad (2)$$

where  $N$  is the sample size,  $r_1$  and  $r_2$  are the lag 1 serial correlation in each of the two series being correlated and  $N_{\text{ef}}$  is the reduced effective sample size used to estimate degrees of freedom in significance estimation.

To extend correlation analyses, some multiple regression models are estimated (daily data over 1982–2016). The  $t$ -value of each regression coefficient predictor is interpreted to assess the power of a predictor relative to a model in which the predictor is excluded (Afifi and Azen, 1979), giving insights to the way in which different variables identified in the composites combine to explain portions of variance in the predictand.

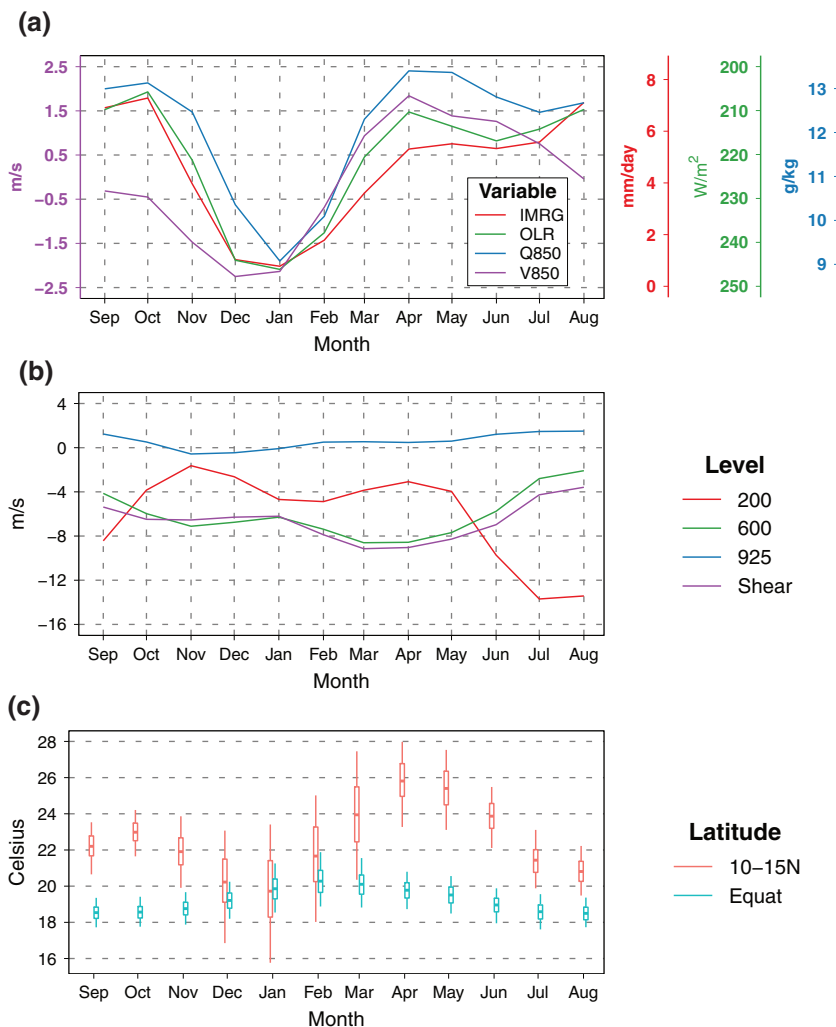


**FIGURE 2** Annual cycle diagnostics over 1982–2016 (except IMERG, 2001–2016). (a) Average over NEC for IMERG precipitation (IMRG), outgoing longwave radiation (OLR), 850-hPa specific humidity (Q850) and meridional wind (V850). (b) Average over NEC for zonal wind at 200-, 600-, and 925-hPa levels, along with 925- to 600-hPa shear (sign reversed for ease of comparison). (c) Temperature at 850 hPa averaged over the longitudes of NEC for 10–15°N (N34 in Figure 1) and equatorial latitudes (S34). Each month is plotted as a box-whisker of daily values showing 50 percentile (mid-point), 25–75 percentile range (box) and 5–95 percentile range (whisker extents) [Colour figure can be viewed at [wileyonlinelibrary.com](http://wileyonlinelibrary.com)]

## 2.3 | Context of North Congo climatology

The NC dry season is clearly distinguished in annual cycles of OLR, IMERG precipitation, low-level meridional wind (northerly during driest months) and low-level moisture (Figure 2a for NEC). It shares many common aspects with conditions at similar latitudes to the west of NC (Maranan *et al.*, 2018). As shown in Jackson *et al.* (2009), in the approximate vicinity of NC, the number of MCSs (and associated rainfall) grows substantially from a minimum in December–January through to April, when Figure 2b shows there is greatest 925- to 600-hPa vertical shear, a potential factor favouring stronger systems (e.g., Rotunno *et al.*, 1988). The increased shear is consistent, through thermal wind balance, with the Sahel – Equator low-level temperature gradient (Figure 2c). The daily variability of low-level temperature near 10–15°N is very high during winter months (Figure 2c), and is considered a key feature for the synoptic sequences addressed in this article.

The domain NEC (Figure 1) is similar to T18. Especially when considering teleconnections to trough indices, a natural extension of interest emerges into the domains westward from NEC (i.e., Northwest Congo (NWC), East Guinea Coast (EGC), and West Guinea Coast (WGC), Figure 1), these domains all lying on the northern edge of the main rain belt in boreal winter

(Figure 1). Subsequent analyses may adjust slightly these regional boundaries, but they are considered sufficient to reveal the targeted features.

## 3 | NORTH CONGO RAINFALL AND DAILY LARGE-SCALE SYNOPTIC TELECONNECTIONS

The days of strongest MCS activity in February over NEC were shown in T18 to be accompanied by substantial low-level tropospheric warming broadly extending to the north, using data for 2007–2016. This result is now shown to be present in all boreal winter months (November to March), using strongest convection days revealed by OLR over 1982–2016 (Figure 3) and wettest days revealed by IMERG over 2001–2016 (Figure S4). Furthermore, there is also strong consistency in the extension of warming into southwestern Asia (especially the Arabian Peninsula), with upstream cooler conditions over the Mediterranean and northwestern Africa. Negative temperature anomalies prevail over NC. Generally, through eastern Africa, positive anomalies prevail, though with some month-to-month variation (see also Section 4.4).

In T18, the juxtaposition of NEC convection anomalies and warming to the north, was preceded by a

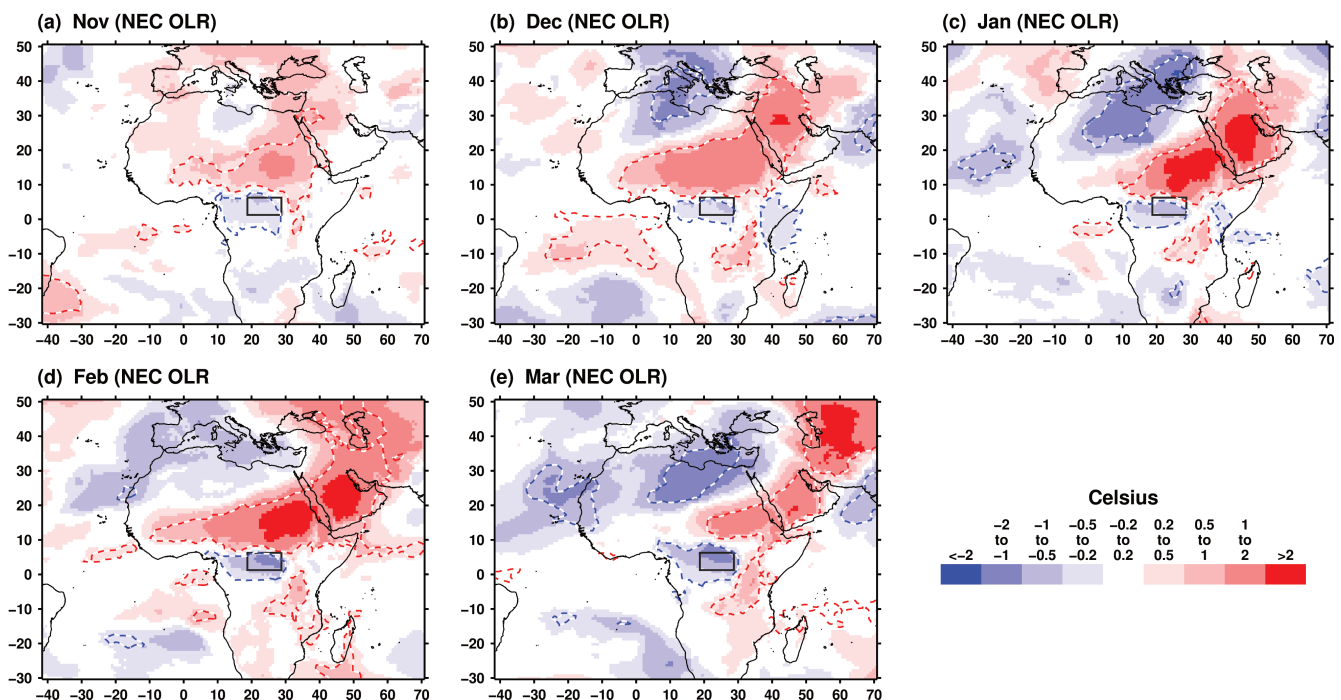


**FIGURE 3** Composite mean anomaly fields of T850 for the wettest (10%) of days 1982–2016 (as indicated by OLR) over NEC (grey box). All results are at zero lag and are calculated separately for (a) November, (b) December, (c) January, (d) February, (e) March. Dashed contour delineates 1% statistical significance (blue dash for negative anomalies, red dash for positive anomalies) [Colour figure can be viewed at [wileyonlinelibrary.com](http://wileyonlinelibrary.com)]

systematic synoptic sequence including northern midlatitude troughs. Qualitatively similar sequences (not shown) are found here for each month November–March, although November is both weaker and less clear in its lag structure. Composite fields for 850-hPa temperature (T850) and Z200 in December–March have been averaged to give a mean representative evolution (from Day –9 to Day 0) for NEC strongest OLR days (Figure 4 left column), NEC wettest days (Figure 4 middle column) and NWC wettest days (Figure 4 right column). Features are remarkably consistent across the columns, suggesting

OLR and IMERG consistency, and NEC and NWC broad-scale similarity.

At Day –9 (Figure 4a–c), all panels indicate a trough over Iberia and up-stream ridge over the Atlantic. Such troughs have previously been associated with downstream warming over parts of North Africa (Knippertz and Fink, 2008). From Day –9 to –6, the trough remains in place, with warming growing over central North Africa, and cooling trailing over the northeastern Atlantic and extending into northwesternmost parts of Africa (Figure 4d–f).

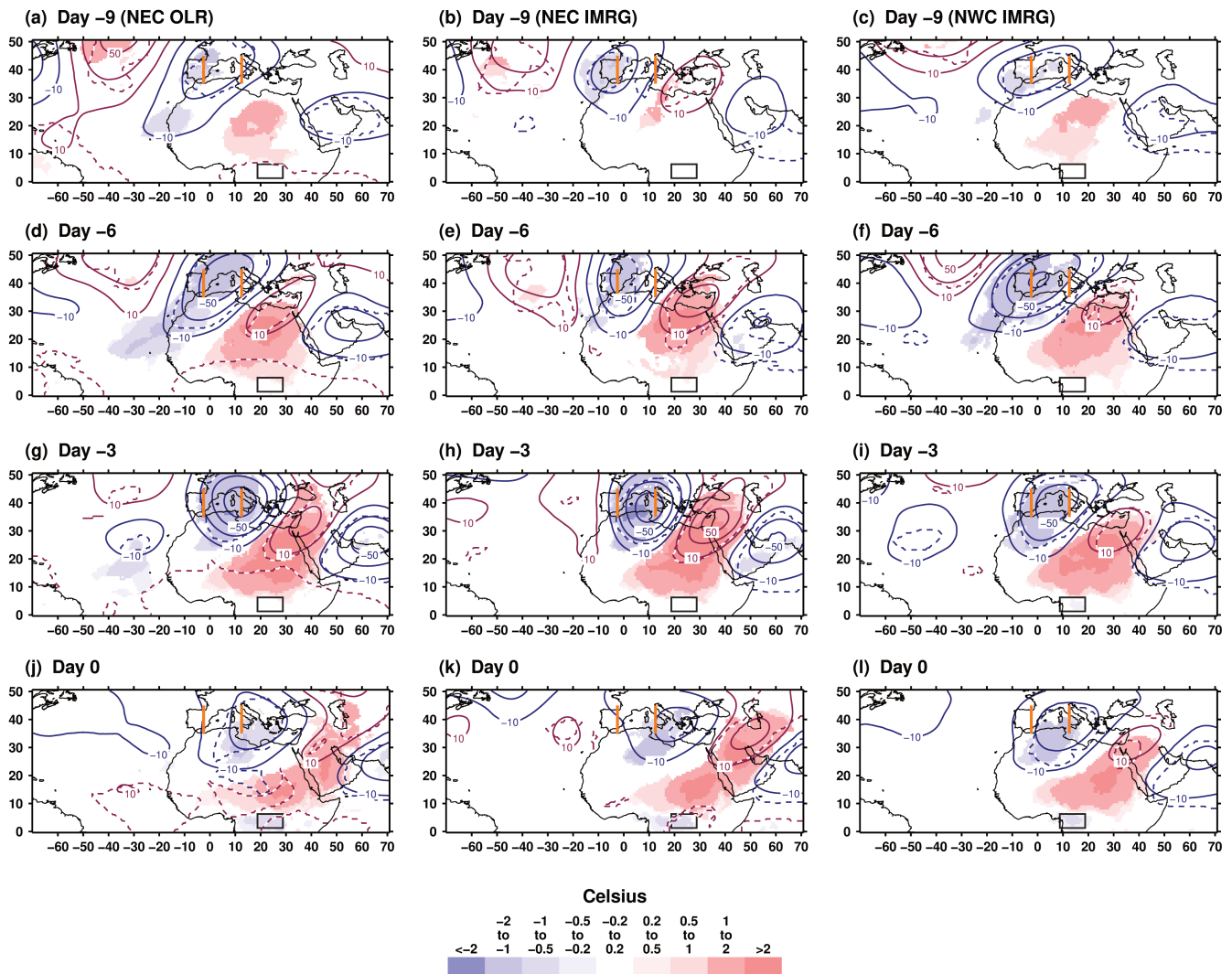


**FIGURE 4** Composite mean anomaly of T850 (shading) and Z200 (contours) at different lead times ahead of the wettest days. All results are calculated individually for each month December to March, and the four composite fields averaged to provide a summary for December to March. (a) NEC (grey box), based on the wettest (10%) of days as indicated by OLR 1982–2016, for Day –9 (9 days before the event). (b) Same as (a) but using IMERG to identify the wettest (20%) of days 2001–2016. (c) Same as (b) but for NWC (grey box). (d–f) same as (a–c) but for Day –6. (g–i) Same as (a–c) but for Day –3. (j–l) Same as (a–c) but for Day 0. Contours of Z200 are for  $\pm 10, 30, 50,$  and  $70$  m, negative anomalies dark blue, positive anomalies dark red. The dashed contours delineate areas where at least 2 of the constituent 4 months attained Z200 significance at 5% level, dashed red for positive anomalies, blue for negative anomalies. T850 shading is restricted to areas where at least 2 of the constituent 4 months attained significance at 1% level. Orange vertical lines mark the trough axes referred to as Iberia ( $2.5^\circ\text{W}$ ) and CMed ( $12.5^\circ\text{E}$ ) in the trough parameter calculation (Equation 1) [Colour figure can be viewed at [wileyonlinelibrary.com](http://wileyonlinelibrary.com)]

For NEC over Day  $-6$  (Figure 4d,e) to Day  $-3$  (Figure 4g,h), the trough transfers eastward to CMed, with now (at Day  $-3$ ) a more clearly defined downstream ridge extending into the northern Arabian Peninsula and trough over the North Arabian Sea (into the Gulf of Oman). The CMed trough—Arabia ridge has similarities (just shifted slightly west) to the Ethiopia Belg dry spell composites in February and March (Bekele-Biratu *et al.*, 2018) as well as Ethiopia rainfall connections in Camberlin and Philippon (2002) which also included January. The implication is that the broad scale synoptic conditions which favour rainfall events in NC tend to favour dry spells over Ethiopia.

Over Day  $-6$  to  $-3$ , T850 anomalies across central and eastern North Africa grow substantially, with anomalies  $>2^{\circ}\text{C}$  extending southeastward to near  $10^{\circ}\text{N}$  over the longitudes of NC (Figure 4g-i). The NEC Z200 midlatitude anomaly pattern for Day  $-3$  (Figure 4g,h) was also found in Vizzy and Cook (2014), but with reversed sign since the focus was on NE Africa winter cold outbreaks, and at their lag Day  $+2$  relative to the start of the cold outbreak.

Over Day  $-3$  (Figure 4g-i) to Day 0 (Figure 4j-l), midlatitude Z200 anomalies actually begin to decay. The T850 signature in midlatitudes also decays. However, just north of NC, positive T850 anomalies continue to evolve (details near NC returned to in Section 5).

In the results for NWC (Figure 4 right column) the axis of T850 anomalies, and especially Z200 anomalies at Day  $-3$  to 0, is shifted slightly westward toward the longitudes of NWC. Also, NWC is slightly ahead of NEC in sequence (more clearly seen in Section 4). Nonetheless, overall, NWC results are very similar to those for NEC, suggesting a common mode of variation is influencing both zones.

Inspection of the lag composites suggests the trough anchor axes over Iberia and CMed (marked on Figure 4) may be key to setting up conditions favourable for NC rainfall. The next section explores the response to strong troughs over these longitudes.

## 4 | AFRICAN RESPONSE TO MIDLATITUDE TROUGHS IN THE ATLANTIC-MEDITERRANEAN SECTOR

### 4.1 | Iberia troughs

First, Iberia troughs are focused upon. They were implicated at the longest lead (up to Day  $-9$ ) in the NC composites (Figure 4). Fields are now composited with Day 0 representing the strongest Iberia trough days (based on

the TP calculation, Equation 1), and following Figure 4, results for each month December–March are combined into one summary result (Figure 5, and with 850-hPa winds, Figure S5). Even 2 days before the strongest trough days over Iberia, a West Africa signature is emerging (Figure 5a). Negative Z200 anomalies are centred just upstream of the Iberia trough axis, while positive T850 anomalies extend ahead of the trough and southward ( $0.5^{\circ}\text{C}$  to about  $15^{\circ}\text{N}$  over  $0\text{--}15^{\circ}\text{E}$ ). The first indication of anomalous convection over southern West Africa (SWA) is consistent with the direct teleconnection mechanism proposed in Knippertz and Fink (2008). At Day 0 (Figure 5b), the warming is growing ahead of the trough, and direct teleconnection to SWA convection (encompassing regions WGC and EGC, Figure 1) is now clearly established with an OLR signature resembling a tropical plume extending northeastward across the Sahara, a feature that often accompanies unseasonable rainfall in the Soudano-Sahelian zone (Nicholson, 1981) and reduced Harmattan winds (Knippertz and Fink, 2008; and see Figure S5).

Over the next days (Figure 5c–f), the area of positive T850 anomalies transfers its main axis southeastward across NE Africa, as in the composites building up to NC rainfall events (Figure 4), and equatorial OLR anomalies emerge further eastward. At first, these track the slowly progressing midlatitude trough and trailing tropical plume. The convection anomalies then become disconnected as the midlatitude anomalies weaken (Figure 5e). By Day  $+7$ , midlatitude Z200 anomalies have decayed, but leaving in place the signature of positive T850 anomalies of  $>1^{\circ}\text{C}$  extending over a vast area of NE Africa and the Arabian Peninsula. Anomalous convection is focused over NEC, extending less strongly westward to near  $10^{\circ}\text{W}$ , but with sharp cut-off near  $30^{\circ}\text{E}$  (Figure 5f). The cut-off matches the geographic Rift Valley highlands divide and here forms a natural climate anomaly boundary.

The composite T850 evolution averaged over  $10\text{--}15^{\circ}\text{N}$  to the north of NEC in each individual month December–March is found to peak over Day  $+4$  to  $+6$ , with very similar overall evolution (red lines, Figure 6a). November and April correspond to transition months. In November, the warming is slower to develop, but is nonetheless at a level of  $+0.5^{\circ}\text{C}$  over Day  $+6$  to  $+8$ , and OLR anomalies over NC do develop as well (not shown). In April, a shorter and weaker T850 anomaly develops (Figure 6a, blue line); this month is quite different overall in its Iberia trough teleconnection to the NC region (not shown). Finally, all other months from May to October do not show any notable warming (dashed lines, Figure 6a).

The Z200 anomalies over Iberia on Day 0 (Figure 5b) tend to migrate somewhat to the east over subsequent days consistent with the climatological upper-level

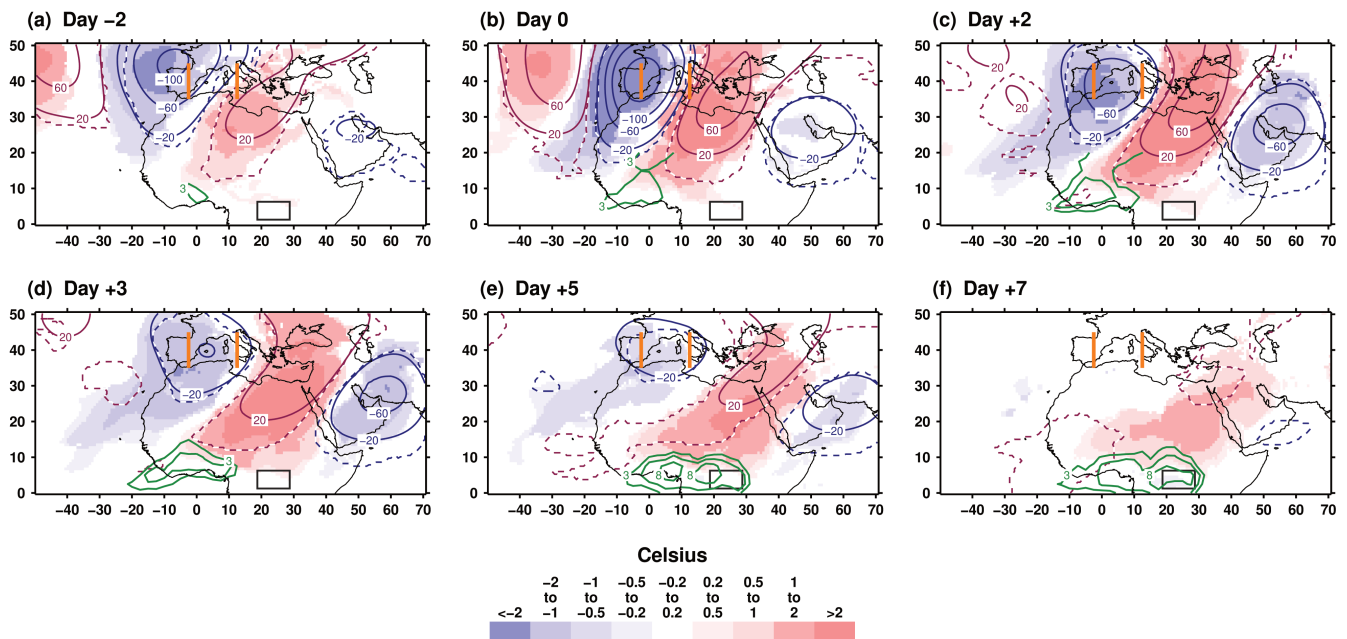


**FIGURE 5** Composite mean anomaly of T850 (shading), Z200 (dark blue/red contours) and negative OLR south of 20°N (green contours) for lags relative to strong Iberia trough days (20% strongest during 1982–2016). All results are calculated individually for each month December to March, and the four composite fields averaged to provide a summary for December to March. Lag in days: (a) –2, (b) 0, (c) +2, (d) +3, (e) +5, (f) +7. Z200 solid contours are for  $\pm 20$ , 60, 100, and 160 m, negative anomalies dark blue, positive anomalies dark red. The dashed contours delineate areas where 2 of the constituent 4 months attained Z200 significance at 5% level. T850 shading is restricted to areas where 2 of the constituent 4 months attained significance at 1% level. OLR contours for –3, –5 and –8 W/m<sup>2</sup>, restricted to the target zone of interest south of 20°N, to highlight the development there of rainfall/convection anomalies (negative sign omitted from OLR contour labels for clarity). Orange vertical lines mark the trough axes referred to as Iberia (2.5°W) and CMed (12.5°E) in the trough parameter calculation (Equation 1). Grey box shows NEC [Colour figure can be viewed at [wileyonlinelibrary.com](http://wileyonlinelibrary.com)]

steering flow. However, they do not develop into the sharp feature near CMed seen in the NC composites (Figure 4). This is discussed further in Section 4.3.

## 4.2 | Troughs at longitude anchor points from the western Atlantic to the eastern Mediterranean: Downstream temperature teleconnections

Iberia troughs are shown in Figure 5 to initially be followed by T850 warming at 10–15°N over the longitudes of NWC, extending subsequently further eastward to the longitudes of NEC. For the six trough anchor points explored stretching from the western Atlantic to the eastern Mediterranean, only Iberia and CMed troughs show such substantial downstream response at 10–15°N (Figure 6b,c).

With a downstream longitude shift of 16° (equivalent to moving from the central axis of Iberia to NWC), CMed troughs actually have a larger response than do Iberia troughs, whereas for a shift of 26°, the response to an Iberia trough is larger. An additional difference is seen in

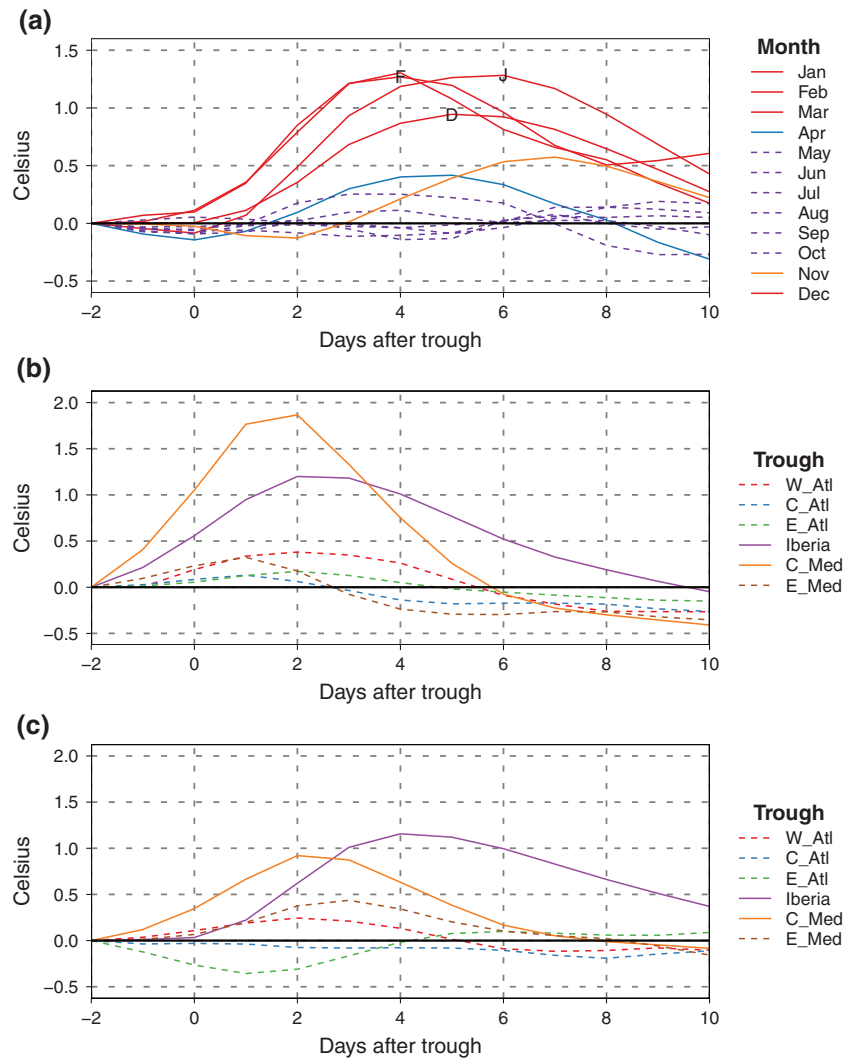
timescale, with the impact of an Iberia trough generally developing slightly more slowly, but persisting longer. While noting these differences in the response to Iberia and CMed troughs, the overall sense in Figure 6b,c supports the hypothesis that troughs with downstream longitudes extending over the continental arid and semi-arid areas of Africa can excite southward penetration and persistence of low-level positive temperature anomalies at low latitudes (to near 10°N), which potentially then influences equatorial convection to the south.

## 4.3 | Iberia and CMed troughs: Independent and interdependent roles in synoptic developments over North Africa

The previous section illustrated how both Iberia and CMed troughs have a statistical expression in T850 to the north of NC. However, from those results, it is not clear if the troughs can impact independently, or if a sequential mobile trough from Iberia to CMed is required. This section addresses this question by defining five subsets of December–March cases, distinguished according to the



**FIGURE 6** Anomalies of T850 (averaged over 10–15°N and 10° longitude blocks) after the strongest Z200 trough parameter values (20% strongest over 1982–2016). All values relative to Day –2, to highlight tendencies. (a) Iberia troughs with T850 measured 26° longitude downstream (i.e., near N34 in Figure 1). Results plotted for each month, highlighting the similarity of December to March (red lines), with partial similarity in November but with delayed warming (orange line). To identify the winter months, maximum values labelled for December (D), January (J) and February (F) (maximum for March almost identical to February). (b) Results combined for December–March T850 anomaly measured 16° longitude downstream from troughs anchored at different longitudes stretching from the western Atlantic (W\_Atl) to eastern Mediterranean (E\_Med) (trough axis longitudes: 47.5°W, 32.5°W, 17.5°W, 2.5°W, 12.5°E, 27.5°E). (c) Same as (b) but for 26° longitude shift [Colour figure can be viewed at [wileyonlinelibrary.com](http://wileyonlinelibrary.com)]



evolution of Iberia and CMed trough parameter values (see Table 1). Inspection of composites of full fields suggested an effective summary may be obtained by considering T850 averages formed over the 10–15°N zones in Figure 1, and with OLR averaged over the OLR domains shown in Figure 1.

The background climate setting is for, on average, a mobile westerly regime, such that troughs have a (modest) tendency to transition from Iberia to CMed. But this average tendency disguises a large range of possible outcomes, as illustrated by the relatively large sample size of each subset (Table 1).

#### 4.3.1 | Subset 1 (Iberia trough, subsequent 5-days CMed neutral)

These results are designed to illustrate how Iberia troughs alone (with conditions subsequently neutral

downstream) extend their influence to the longitudes of NEC. The distinctive feature of the composites (Figure 7a,b) is the relatively slower timescale over which T850 and OLR anomalies develop. Initially, the strongest temperature anomalies are in the western zone N12, but out to Day +11, statistically significant positive anomalies are present across all temperature indices. There is strong initial enhanced convection in EGC and WGC, which eventually spreads to NEC (significant at 1% level for Day +6 to +10).

#### 4.3.2 | Subset 2 (CMed trough, prior 5-days Iberia neutral)

In contrast to subset 1, T850 anomalies are strongest over eastern parts of the domain, peaking higher (almost +2°C) but on a relatively shorter timescale. Associated anomalies of convection are now mostly confined to

**TABLE 1** Subsets to distinguish Iberia and CMed trough teleconnection patterns according to the evolution of Iberia and CMed trough parameter values

Subset number	Sample size	First condition	Second condition
1	266	Iberia trough	CMed neutral: Following 5-days CMed mean value resides in middle tercile
2	257	CMed trough	Iberia neutral: Previous 5-days Iberia mean value resides in middle tercile
3	282	Iberia trough	CMed ridging: Following 5-days CMed mean value less than median value
4	285	CMed trough	Iberia ridging: Previous 5-days Iberia mean value less than median value
5	256	Iberia trough	CMed Troughing: Following days 2–4 CMed mean value above 20th-percentile

*Note:* The first condition is always a single day 20th-percentile event (either Iberia or CMed trough). The second condition defines the sequence type to focus upon (based on multiple-day averages of Iberia or CMed trough parameter values). All 4,244 days, December–March 1982–2016 are pooled together for the analysis, so a 20th-percentile cut-off initially contains a sample of 849 days. The secondary condition further reduces sample size to the values shown (but still large samples for estimating the associated composite mean conditions, see Figure 7). Note the samples are defined to address specific hypotheses on Iberia–CMed sequencing, and are not required to be independent (with some days falling into more than one sample).

NEC, and mirror the shorter T850 anomaly timescale (significant at 1% for Day +2 to +5). Indeed, the propagation of T850 anomalies is much clearer in subset 1 with, for example, greater spread of the curves along  $0.5^{\circ}\text{C}$  from Day –1 (achieved by N12) to Day +3 (achieved by N45). Therefore, the independent CMed (Figure 7c,d) and Iberia (Figure 7a,b) signatures have differences, but they do both ultimately lead to warming north of NEC and anomalous convection over NEC.

#### 4.3.3 | Subset 3 (Iberia trough, subsequent 5-day CMed ridging)

The impact is now confined to modest initial enhanced convection over WGC (Figure 7f) and modest positive T850 anomaly, only extending eastward to N12, with T850 anomalies at the longitudes of NC actually negative (Figure 7e). Therefore, unfavourable circulation over CMed can shut off the Iberia influence on NC.

#### 4.3.4 | Subset 4 (CMed trough, prior 5-day Iberia ridging)

Compared to when prior conditions were neutral (Figure 7c,d), the T850 and OLR anomaly sequences over Day 0 to +5 maintain a similar pattern (Figure 7g,h). Therefore, CMed troughs may influence NEC even if upstream conditions over previous days were not favourable, although the magnitude of impact is somewhat reduced.

#### 4.3.5 | Subset 5, (Iberia troughs, subsequent CMed 2–4 days strongly troughing)

For 1–5 days after a strong Iberia trough (20th-percentile), there is a significantly increased likelihood of a strong (20th-percentile) CMed trough (1% significance based on chi-square test). Here, the following days 2–4 are focused upon, consistent with the mean timing sequence seen in Figure 4 (although results are similar if a CMed window of 1–5 days is used). The subset illustrates the combined influence of Iberia and CMed troughs. Compared to the other subsets, T850 anomalies are strongest (peaking  $>2.5^{\circ}\text{C}$ ) and maintain the highest values over more days. Similarly, OLR anomalies across EGC, NWC, and NEC display enhanced response, especially for NEC.

#### 4.4 | CMed trough linkages in each month November–March

Figures 5 and 7 combined December–March results into a single seasonal summary; however, for CMed troughs, rather stronger variation in synoptic teleconnections month by month is found, and this is illustrated in this sub-section. Consistent with Figure 7a–d, the timescale of impact into NC is shorter and sharper for CMed troughs (compared to Iberia troughs), with Day +3 providing an overall summary (Figure 8). The composites use the full set of strong CMed trough days, to provide the largest sample. This will also weakly include the impact of Iberia

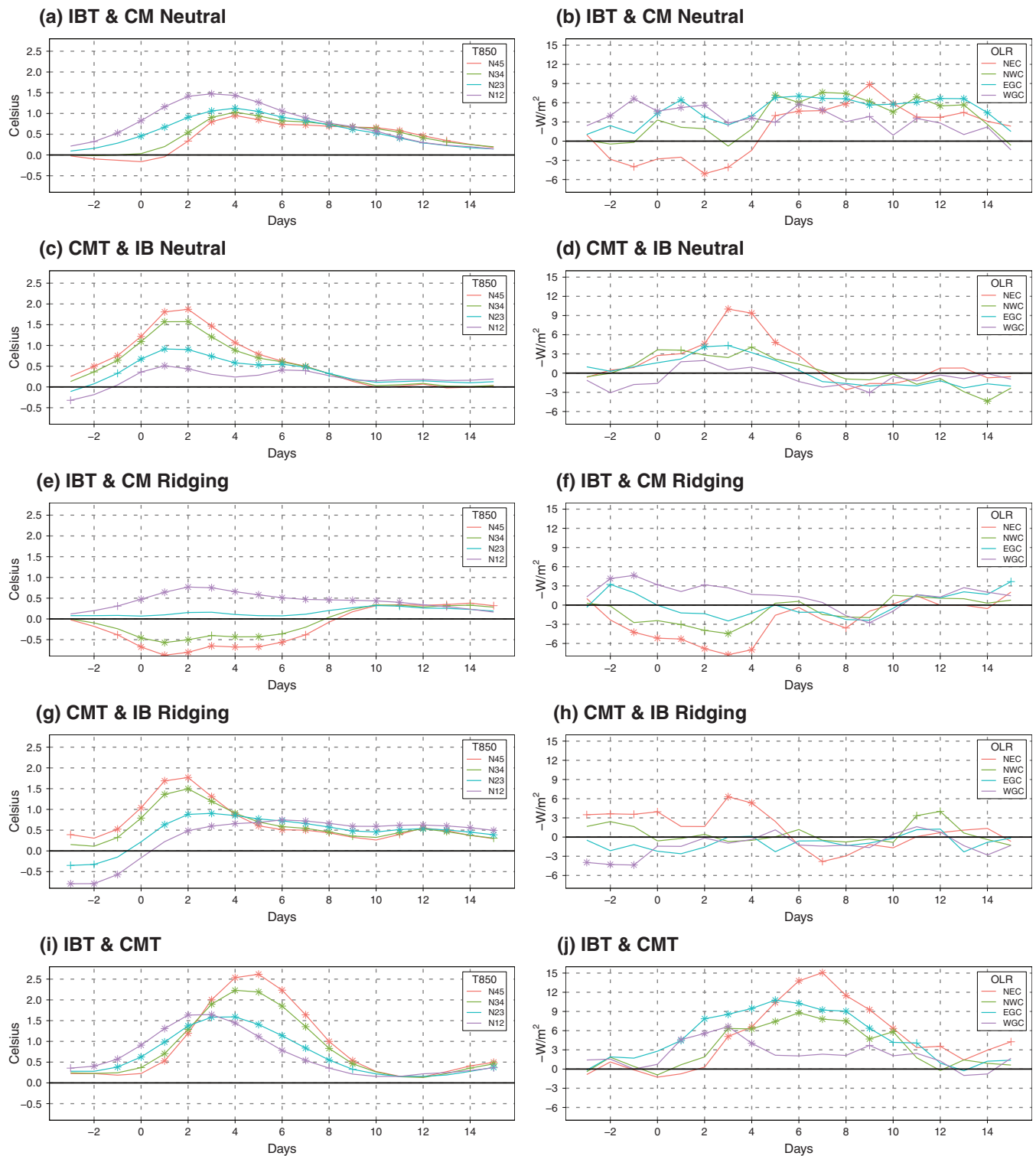


**FIGURE 7** Lag composites for subsets of strong Iberia and CMed trough days (see Table 1 for definition of the subsets). (a) Composite mean anomalies of T850 at 10–15°N (lags Day –3 to Day +15) for a subset of Iberia trough days December–March 1982–2016 (Subset 1 in Table 1, Iberia troughs followed by neutral CMed conditions). Anomalies significant at 1% (5%) are indicated by asterisk (plus). Target T850 regions (N45–N12) are shown on Figure 1. (b) Same as (a) but for OLR anomalies (units  $-W/m^2$ ) stretching from NEC to WGC (see Figure 1). (c,d) Same as (a,b) but for CMed troughs Subset 2 in Table 1 (CMed troughs preceded by neutral Iberia conditions). (e,f) Same as (a,b) but for Iberia troughs Subset 3 in Table 1 (Iberia troughs followed by ridging CMed conditions). (g,h) Same as (a,b) but for CMed troughs Subset 4 in Table 1 (CMed troughs preceded by ridging Iberia conditions). (i,j) Same as (a,b) but for Iberia troughs Subset 5 in Table 1 (Iberia troughs followed by strong CMed trough conditions). Acronyms in the panel headings: CM, CMed; CMT, CMed trough; IB, Iberia; IBT, Iberia trough [Colour figure can be viewed at [wileyonlinelibrary.com](http://wileyonlinelibrary.com)]

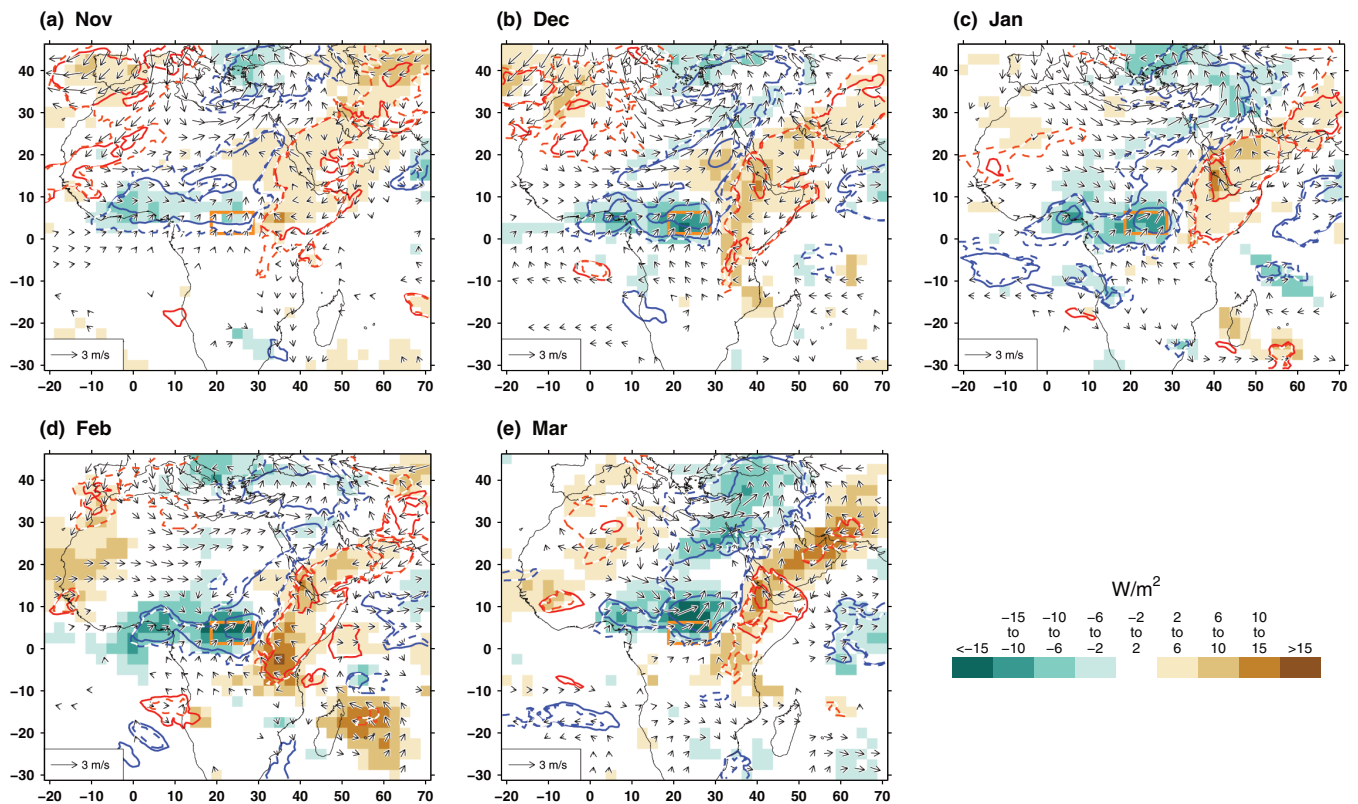


**FIGURE 8** Composite anomaly fields at Day +3 after a strong CMed trough (20% strongest 1982–2016). (a) November, (b) December, (c) January, (d) February, (e) March. Shading is OLR (plotted where achieving significance at the 10% level). Solid contours are 850-hPa specific humidity at  $\pm 0.4$  and  $1.2$  g/kg, positive contours blue, negative contours red. Dashed contour delineates 1% statistical significance, dashed blue for positive anomalies, red for negative anomalies. Vectors are 850-hPa wind, averaged over  $3.75^\circ$  boxes, and vectors only plotted if 50% of the constituent 25 boxes achieved significance at the 10% level in u or v. Patterns over highland areas of East Africa where 850 hPa is below the surface (such that the features shown represent interpolations) are nonetheless found indicative of regional synoptics, since consistent features are seen at 600 hPa (see Figure S6). Orange box shows NEC [Colour figure can be viewed at [wileyonlinelibrary.com](http://wileyonlinelibrary.com)]

troughs, due to the modest statistical tendency for Iberia troughs to precede CMed troughs. Notable OLR and low-level atmospheric features may be summarized from Figure 8 as:

- A very consistent set of anomalies over NC with south-westerly winds, increased moisture and enhanced convection. The latitude of these anomalies migrates slightly with the annual cycle, shifting southward in January (Figure 8c), relative to November (Figure 8a), and March (Figure 8e). The complex is effectively representing a northward extension of the broader Congo Basin rainfall/convection zone (Figure 1). All months display a boundary at about  $30^\circ\text{E}$  for the zone of enhanced convection and low-level moisture, a boundary consistent with T18 and also seen in other studies for March–May (e.g., Jackson *et al.*, 2019; Finney *et al.*, 2020).
- In all months, extending northeast from NC, a zone of enhanced moisture reaches across the Sahara into the eastern Mediterranean and Middle East, connecting with the remnants of the strong CMed trough (also seen at 600 hPa, Figure S6). This resembles a type of tropical plume and requires further analysis to assess similarity with more studied tropical plumes, such as ones coupled to the Iberia trough and rainfall over SWA (e.g., Figure 5c).
- East of NC, moisture and convection anomalies reverse sign, becoming significantly negative, with some variation in details by month. The anomalies extend northeast, into Ethiopia (especially in February and March), and also into southern parts of the Arabian Peninsula continuing to border regions of South Asia.
- The negative convection and moisture anomalies also extend broadly through East Africa, notably in December (end of the Short Rains) and February–March (early Long Rains). Especially in February, the southward extension reaches  $10^\circ\text{S}$  and also connects to a perturbed South Indian Convergence Zone (Cook, 2000; Lazenby *et al.*, 2016). Clear expression,

with some month-to-month evolution, is also seen in wind, moisture and convection anomalies connecting southwestern Asia and the northwestern Indian Ocean.

- Upstream of the CMed trough, generally negative moisture anomalies are found over the Maghreb/broad northwestern Africa domain. Anticyclonic wind anomalies prevail especially in November, December and March.

#### 4.5 | Discussion on the trough impacts

These results motivate better understanding of the Iberia and CMed trough variability. Near Iberia, troughs often have a southwest-northeast orientation, and can become quasi-stationary with a tropical plume of moisture ahead of the trough. Such features are known to preferentially occur on the eastern side of the North Atlantic extending toward Iberia (Fröhlich *et al.*, 2013). Trough transition from Iberia to CMed longitudes may occur as the long-wave upper-level regime transitions from quasi-stationary to a progressive Rossby wave.

CMed troughs can, however, occur independently and may have different orientations. Indeed, in Z200 teleconnection composites for CMed troughs (not shown), the mean upstream origin (e.g., Day  $-3$ ) tends to be centred not over Iberia but much further north, with subsequent track southeastward into the CMed domain at Day 0. The same composite sequence, but with reversed sign, is associated with NE Africa winter cold events (Vizy and Cook, 2014). The northwest-southeast arrangement resembles a Rossby wave train entering the broader domain (Knippertz, 2007; Van der Wiel *et al.*, 2015), with similarities to the proposal of Matthews (2012) on the excitation of the South Pacific Convergence Zone as the time-averaged composite of a sequence of mobile, Southern Hemisphere troughs. This could motivate development of a tailored trough parameter with northwest-southeast orientation.

It is also possible that previous sequences of midlatitude troughs precondition the continental land mass to NE Africa warming and NC precipitation events (Knippertz and Fink, 2009). In the process of exploring such a possibility, it will also be valuable to assess whether large-scale conditions (such as sea-surface temperature patterns or Madden-Julian Oscillation activity) favour multiple sequences of the Iberia and CMed troughs in given years. These possibilities are hinted at by the fact that in some trough and NC composites, modest (but significant) warming over North Africa is already in place prior to the composite sequence beginning.

Furthermore, the possibility of conditions over Africa feeding back to reinforce the midlatitude sequences cannot be ruled out.

## 5 | NORTHERN CONGO DRY-SEASON CONVECTION/RAINFALL AND NEARBY ATMOSPHERIC DIAGNOSTICS

This section assesses in more detail the Sahara temperature—NC link. Composite fields for NEC strong events over December–March are initially focused upon (Figure 9, Section 5.1). However, the majority of findings hold also, with minor adjustments, for November and for NWC, which are included in the summary statistical analyses for all days (Section 5.2).

### 5.1 | Composite fields

At low levels (Figure 9 left column), just to the north of NEC, the transition from Day  $-4$  to  $-2$  sees intensifying anomalous north-to-south temperature gradient, with the  $2^{\circ}\text{C}$  isotherm near  $10^{\circ}\text{N}$  at Day  $-2$  (Figure 9c). Over NEC and to the north, there is an anomalous southerly wind, and low-level moisture build-up. These features resemble those found by Knippertz and Fink (2008) in dry season rainfall events further west over SWA, and imply adjustment of the nearby heat low at these longitudes (Lavaysse *et al.*, 2009) permitting southerly winds and associated moisture to penetrate further north than normal and precondition the environment for unseasonable rainfall events. Averaged over NEC, the moisture anomaly is at a maximum at Day 0, and anomalous 925-hPa winds turn to have a strong westerly component, over and to the south of NEC. A negative temperature anomaly develops over NEC, consistent with a response to the precipitation.

At mid levels (600 hPa, Figure 9 right column), anomalous moisture is already in place to the north of NEC at Day  $-4$  (again resembling a tropical plume orientation). By Day 0, the moisture anomaly moves eastward in its northern section, and also extends southward. Low mid-level moisture and descending motion are features of the rainfall-suppressing time-mean climatology at this time of year over and just to the north of NEC (Dezfuli, 2017); the presence and development of these positive mid-level moisture anomalies (Figure 9) is therefore a candidate to contribute to NEC events. In addition, 600-hPa easterly wind anomalies are found on the southern flank of the moisture plume, and these intensify at Day 0 (Figure 9f) over NEC (consistent with T18).

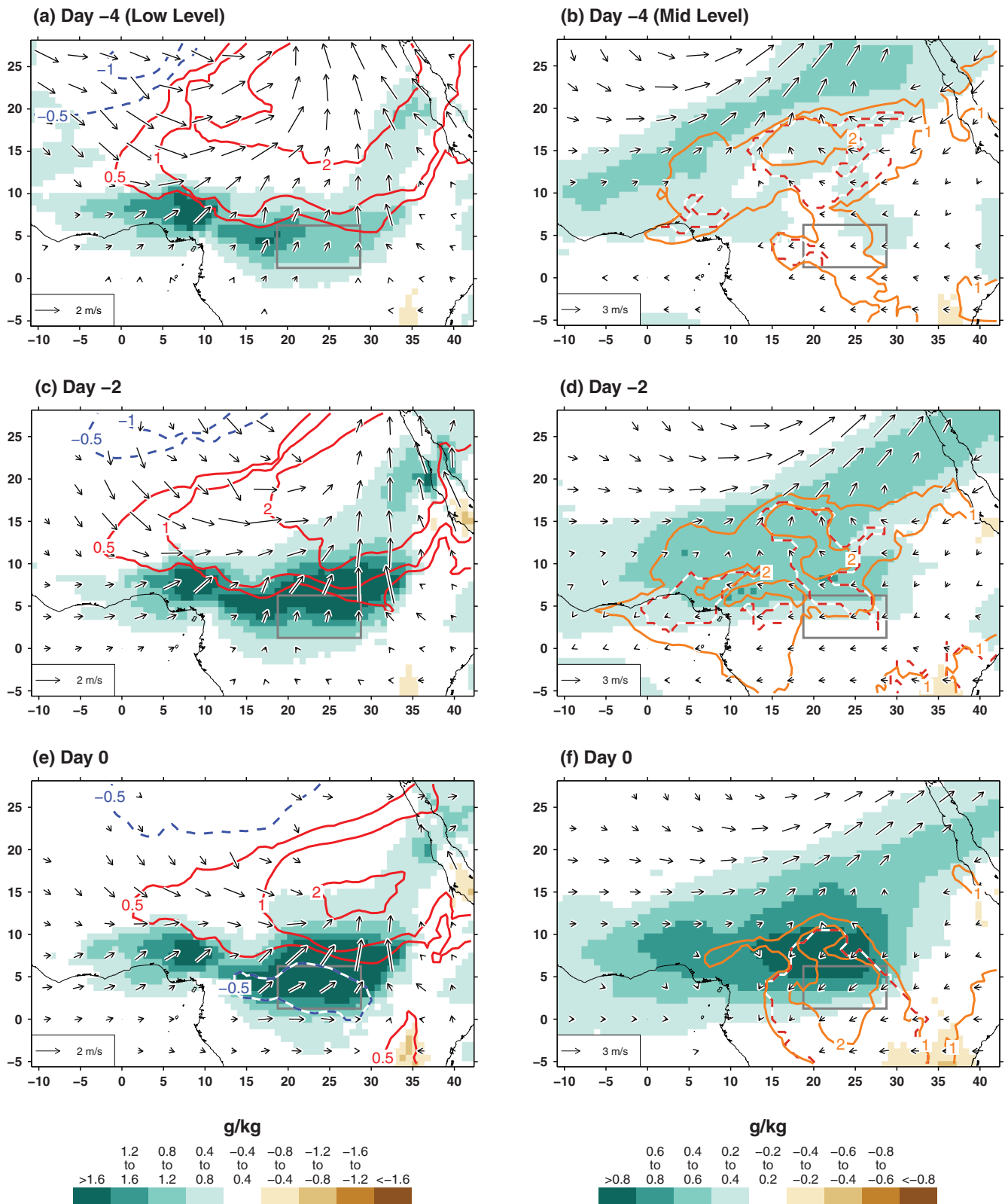


**FIGURE 9** Composite mean anomaly for the 10% of wettest NEC days (as indicated by OLR) over 1982–2016 for December–March (months combined as in Figure 4). (a) Day -4 fields of 925-hPa specific humidity (shading) and wind (vectors) along with T850 (contours at  $\pm 0.5$ , 1, and  $2^\circ\text{C}$ , negative dashed blue, positive solid red). Specific humidity shading only for areas where at least 2 of the 4 constituent months are significant at 5% level. Vectors are 925-hPa wind averaged to  $3.75^\circ$  boxes, and vectors only plotted if 50% of the constituent 25 boxes achieved significance (2 of 4 months at 5%) in u or v. (b) Same as (a) but for 600-hPa specific humidity and wind, along with positive contours (orange) of 925- to 600-hPa zonal wind vertical shear, contours at +1 and +2 m/s, with dark orange dashed contour delimiting areas where all 4 months are assessed significant at the 5% level. (c,d) Same as (a,b) but for Day -2. (e,f) Same as (a,b) but for Day 0. Grey box shows NEC [Colour figure can be viewed at [wileyonlinelibrary.com](http://wileyonlinelibrary.com)]

The anomalous mid-level easterly coupled with near-surface westerly at Day 0, implies positive vertical shear anomaly over NEC (Figure 9f), a candidate to intensify convection (e.g., Browning and Ludlam, 1962; Rotunno *et al.*, 1988; Alfaro, 2017). The vertical shear anomaly is consistent through thermal wind expectation with the anomalous north-south low-level temperature gradient (Figure 9). The way in which such dynamics operate as the Equator is approached also requires assessment in completing such arguments in this setting. The issue is returned to in a statistical sense below.

## 5.2 | Statistical summary over all days

The peak composite T850 anomaly to the north of NEC at 10–15°N is found at a lead of 2-days, located north-north-east of NEC (Figure 9c) and this result is reproduced in terms of correlation over all days (Table 2,

**TABLE 2** Correlation of daily OLR Index (NEC or NWC) with daily T850 Indices (see Figure 1 for locations)

Lead	NEC			NWC		
	N12	N34	N45	N12	N23	N45
4	.32	.34	.32	.34	.32	.29
3	.33	.41	.41	.37	.37	.34
2	.30	.45	<u>.46</u>	.36	<u>.39</u>	.37
1	.23	.41	.43	.32	.38	.36
0	.15	.31	.32	.26	.33	.32

*Note:* Lead is in days, T850 leading OLR. OLR is multiplied by  $-1$  so it becomes a proxy for rainfall/convection. All indices expressed as daily anomalies. Strongest correlation underlined, in each case, lead of 2 days, T850 index located north-north-east of the target OLR region. Analysis uses December–March 1982–2016, total sample size 4,244 days. All correlations remain statistically significant with  $p$ -value  $<.0001$  after estimating effective sample size due to serial correlation ( $r_1$  values NEC = .53, NWC = .46, T850 indices range .90–.94, effective sample size estimated  $>1,400$  for all correlations shown).

**TABLE 3** Intercorrelation of key variables at zero lag (daily December–March anomalies)

	V925 Q925	V925 G850	Q925 G850	Q925 OLR	U925 OLR	S925 OLR	Q600 OLR
Over NEC	.81	.81	.77	.52	.43	.31	.41
Over NWC	.77	.73	.75	.45	.35	.22	.39

*Note:* Variables are averaged over the domains of NEC or NWC (see Figure 1) (except: Q600, which uses the longitudes of NEC/NWC but is offset norward to extend over 5–10°N, consistent with the offset in Figure 9; G850 is the T850 meridional gradient defined in Figure 1). S925 (vertical shear) is the difference in zonal wind between 925 and 600 hPa. Sample size as Table 2. All correlations remain statistically significant with  $p$ -value  $<.0001$  after estimating effective sample size due to serial correlation ( $r_1$  values for Q925 and G850 variables .91–.93, U, V, S, and Q600 variables .71–.84, effective sample size estimated  $>300$  for Q925 vs. G850,  $>600$  for correlations involving V,  $>1,400$  for correlations involving OLR).

T850 index N45,  $r = .46$ , based on daily December–March indices 1982–2016). For NWC, maximum correlation is at the same lead and north–north-east orientation (Table 2, T850 index N23,  $r = .39$ ). These T850 relationships are almost identical at a lead of 1-day (Table 2, and seen in composites, not shown).

At zero-lead, the strongest linkages with OLR are found with local atmospheric diagnostics (over the NEC and NWC domains, Table 3). A primary covarying set of features (Table 3) is 925-hPa meridional wind (V925), moisture (Q925), and north-south T850 gradient (G850, formed from the T850 domains defined in Figure 1). Of these three variables, it is Q925 that has highest correlation with the OLR indices (Table 3,  $r = .52$  for NEC, .45 for NWC), although OLR also strongly correlates with V925 and G850 (not shown).

The intercorrelation of Q925, 925-hPa zonal wind (U925) and 600-hPa moisture (Q600) is relatively low (mean  $r = .36$ ) and they are found to each account for substantial additional fractions of daily OLR variance (Table 4,  $t$ -values high for all three variables). This model holds when fitted in each individual month, including November (Table S1).

Vertical shear, approximated here as the difference in zonal wind between 925 and 600 hPa (S925), also has significant correlation with OLR (Table 3), but not as strong as U925. Indeed, S925 is unable to significantly enter the regression model (Table 4), once U925 is entered. It is, however, still possible that shear is strongly contributing to some rainfall events. Targeted moisture budget and stability assessments including sub-daily data and atmospheric model experiments can be expected to provide insights into the role of the low-level and mid-level fluctuations revealed in the statistical analyses, with a different balance of factors likely for different rainfall types (Maranan *et al.*, 2018), including stronger role for low-level temperature gradients a few hours before rainfall types involving MCSs (consistent with T18 and Klein and Taylor, 2020).

Predictand	Q925		U925		Q600		Multiple correlation
	Coeff	tval	Coeff	tval	Coeff	tval	
NEC	2.91	16.57	4.92	16.65	5.80	16.74	.59
NWC	3.80	15.20	5.31	13.51	5.74	17.39	.53

Note: Analysis includes all days December–March 1982–2016, and all indices expressed as daily anomalies. Regression coefficient (Coeff) and associated *t*-value (*tval*) is shown for each predictor, along with the overall model multiple correlation fit.

Predictand	T850		EGC		Multiple correlation
	Coeff	tval	Coeff	tval	
NEC	4.01	28.41	.19	12.31	.49
NWC	3.72	22.38	.17	10.75	.42

Note: Predictor T850 (°C) indices (N45 for NEC and N23 for NWC) and OLR index (EGC,  $-W/m^2$ ) located on Figure 1. Analysis period as in Table 4. The multiple correlation clearly beats the 2-day persistence correlation, which for NEC  $r = .27$ , NWC  $r = .19$ .

Each variable in the specification equation in Table 4 does have some modest predictive capability for OLR, when explored at lead times of a few days. However, the T850 indices dominate in prediction models, strongly suggestive that T850 is a precursor for the key features that deliver rainfall. For example, predicting NEC OLR at lead of 2 days, the predictive correlation for Q925, U925 and Q600 is .35, .15, and .24, respectively, but these drop to partial correlations of .09,  $-.07$ , and .12 when N45 (lead of 2 days) is controlled for, confirming they have no ability of substance to explain NEC OLR variability that is independent of the N45 T850 index.

One additional feature that is robust with a lead of a couple of days is OLR to the west. The illustration for lead of 2 days in Table 5 uses OLR measured over the EGC domain (plus T850 indices) to predict both NEC and NWC. The T850 indices are the dominant predictor, but EGC significantly raises the skill of the model (evident through inspection of predictor *t*-values, and the model is found to hold for all months December–March, see Table S2). These results imply some additional independent lagged linkage between EGC and NC, reinforcing the idea of a modest internal atmosphere tendency for eastward migration of rainfall. This supports a small role for Iberia troughs influencing NC rainfall through the direct Iberia trough–EGC linkage (Knippertz and Fink, 2008). The relative importance of this secondary pathway may best be assessed through numerical model experimentation, especially given that migration eastward of T850 near  $10$ – $15^\circ N$  is also occurring (e.g., Figure 5). Indeed, the main result of this diagnostic section is to support the primary pathway for upper-level troughs through their impact on T850

**TABLE 4** Specification regression equation (zero lead) for daily OLR ( $-W/m^2$ ) over the NEC and NWC domains, using predictors Q925 (g/kg), U925 (m/s), and Q600 (g/kg) (domains as defined in Table 3)

**TABLE 5** Prediction regression equation (2-day lead) for OLR ( $-W/m^2$ ) over the NEC and NWC domains

anomalies in areas that anticipate NC rain events and the associated key atmospheric features.

## 6 | MONTHLY/SEASONAL MEAN EXPRESSION FOR CLIMATE ANALYSES

The above synoptic sequence results are expected to have further relevance through their implications for climate scale variability in the region (as discussed for February in T18). Inspection of Figures 5 and 7 (especially Figure 7b,j) suggests that a time-mean OLR index averaging together EGC, NWC, and NEC may have expression in regional climate anomalies. Teleconnections with such an index (Figure 10a) reveal that monthly-mean enhanced convection through January–March correlates strongly with positive T850 anomalies across NE Africa ( $r > .7$ ), and with low-level southwesterly anomalies emanating from the tropical Atlantic and Congo Basin. These wind features extend further south than the synoptic sequence studied, suggesting an additional role in the seasonal mean anomalies for broader scale fluctuation in the Atlantic-Congo regional system. Links extend eastward through eastern Africa (Figure 10a) into the Indian Ocean, with anomalous winds there extending from  $10^\circ S$  to the Arabian Sea.

Over the northern Arabian Sea there is a strong trough in the Z200 correlation field (Figure 10a); indeed, this is a relatively stationary feature in the synoptic sequence (e.g., only small migration eastward over Day  $-9$  to  $-3$  in Figure 4). This contrasts with the transition from Iberia to CMed in Figure 4, which likely leads to a



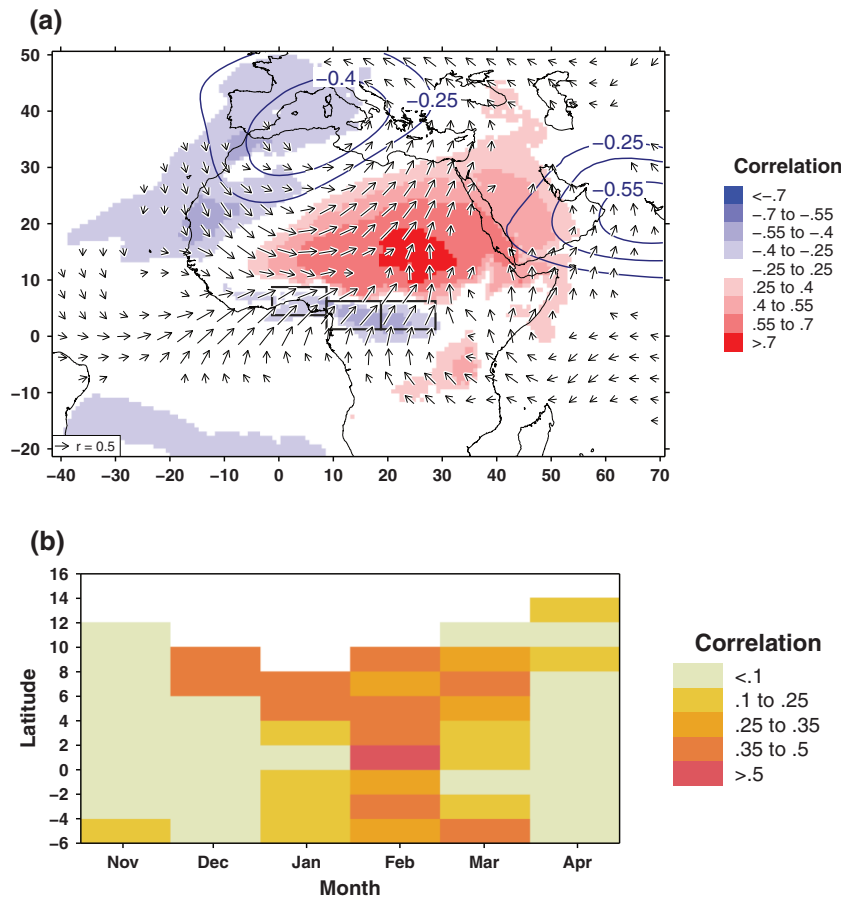


**FIGURE 10** (a) Correlation of monthly mean anomalies of OLR averaged over the grey box domains shown (i.e., averaging NEC, NWC, and EGC) with monthly mean anomalies of T850 (shading), 850-hPa winds (vectors) and Z200 (contours). Results are for January, February, and March 1982–2016, so each correlation is based on  $35 \times 3 = 105$  pairs of values (all anomalies expressed relative to the given month's climatology), 1% significance  $r = .25$ . Correlation contours (Z200) are at  $\pm 0.25$ , 0.4, and 0.55; negative contours dark blue, no positive contours meet the 0.25 threshold. Vectors are formed from the u and v wind correlation, with values averaged to  $3.75^\circ$  boxes, and only plotted if 50% of the constituent 25 boxes achieved significance at the 1% level in u or v. (b) relating monthly mean intense trough activity over CMed with monthly mean areal coverage of intense tropical MCSs over 0–15°E (MCS definition follows Taylor *et al.*, 2018). Correlations are by month over 1982–2016 (so each correlation based on 35 pairs of values, 5% significance  $r = .33$ ). Trough activity is the count of strong CMed trough days each month. MCS activity is mean fractional area covered with intense ( $-70^\circ\text{C}$  threshold) contiguous areas of cold cloud sampled daily at 1800 UTC. The MCS monthly mean is formed with a 5-day offset (i.e., for 6th of target month to 5th of following month) so that MCS activity lags the trough index by 5 days [Colour figure can be viewed at [wileyonlinelibrary.com](http://wileyonlinelibrary.com)]

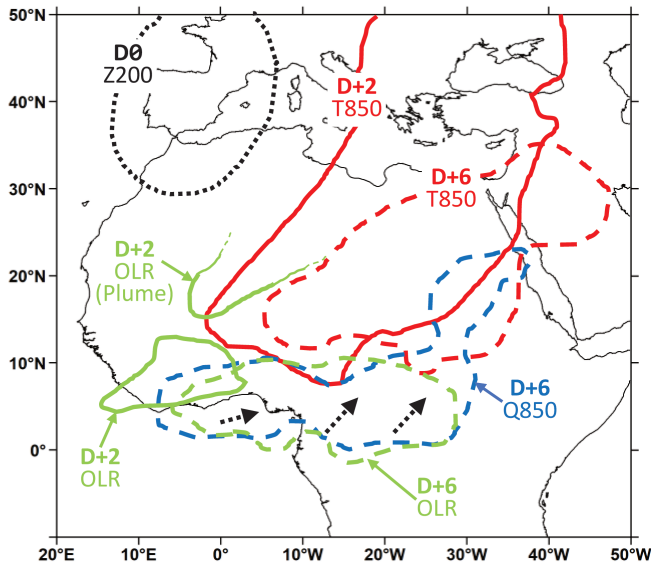
damping and spreading of monthly mean Z200 correlation across Iberia and CMed longitudes in Figure 10a. Monthly mean correlations with December (Figure S7a) are much reduced and with different pattern, requiring further investigation.

This work was initially motivated by the analysis of strong MCSs over NC as revealed by METEOSAT (T18). At the monthly scale and averaged over 0–15°E, such MCS indices do link with CMed trough activity (Figure 10b), here measured using a count of the number of strong (fifth-percentile) CMed troughs in each month. Such an index may be considered a simple initial step in developing a summary statistic for diagnostic analysis. Significant connections are found for December–March,

generally over 4–10°N (Figure 10b), extending notably further south in February. When MCS activity is averaged over 0–28°E (i.e., including the longitudes of NEC), results are overall similar (Figure S7b), though with slightly less emphasis on December–January, and more on February–March (the lag 1 serial correlation of the CMed index is  $<.1$  for all months except March, when  $r_1 = .55$ ).

The Iberia and CMed trough indices have so far been found to have only very modest linkages with other atmospheric teleconnection indices for the region (e.g., Barnston and Livezey, 1987). At monthly scale over 1982–2016, the NAO has no notable correlation with monthly mean values of either the Iberia or CMed

## (a) Iberia



## (b) CMed

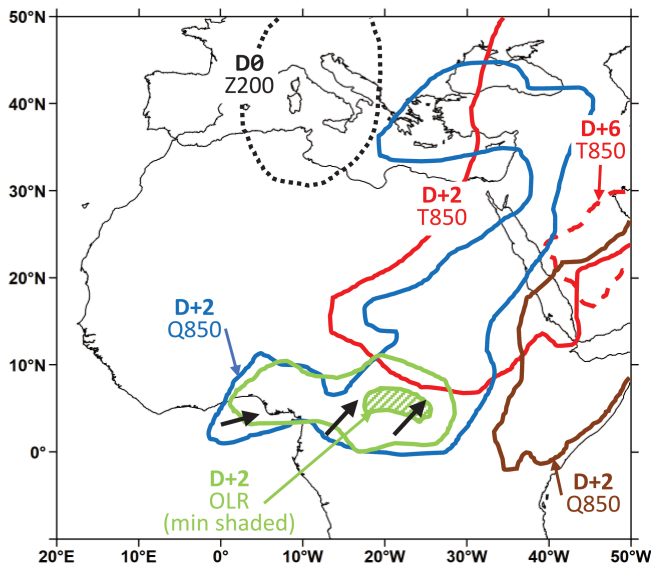


**FIGURE 11** (a) Schematic based on composite anomalies using the strongest (20%) Iberia trough days December–March 1982–2016. Anomalies depicted: Z200 of  $-100$  m at Day 0 (dotted black); T850 of  $+1^{\circ}\text{C}$  at Day +2 (solid red) and Day +6 (dashed red); OLR of  $-5$   $\text{W}/\text{m}^2$  at Day +2 (solid green) and Day +6 (dashed green); Q850 of  $+0.4$   $\text{g}/\text{kg}$  at Day +6 (dashed blue). Dashed black vectors depict low-level wind anomaly at Day +6 (not to scale). (b) Same as (a) but for CMed trough, and with: at Day +2 OLR includes  $-10$   $\text{W}/\text{m}^2$  (shaded green); black vectors are solid for day +2; Q850 includes  $-0.4$   $\text{g}/\text{kg}$  (solid brown, Day +2). The juxtaposition of positive and negative Q850 anomalies extends to mid levels (600 hPa, not shown). At Day +6, the area of T850 anomaly of  $+1^{\circ}\text{C}$  has contracted, now in southwestern Asia and extending less far south, with relatively small residual OLR and Q850 anomalies (not shown) south of  $20^{\circ}\text{N}$ , in similar locations to those found at Day +2 [Colour figure can be viewed at [wileyonlinelibrary.com](http://wileyonlinelibrary.com)]

indices (all  $r < |.2|$  for November–March, and at daily scale, all  $r < |.1|$  for synoptic lags  $\pm 10$  days). Similar low NAO linkages were also found with tropical plume frequencies over the North Atlantic (Fröhlich *et al.*, 2013). However, the East Atlantic/Western Russia (EAWR) mode at monthly scale does correlate at  $-.34$  to  $-.48$  over November–February with the CMed trough index (over 1982–2016, all four correlations are significant at 5%). This is consistent with the observation in T18 that features related to NC partly resembled the EAWR (e.g., Ionita, 2014). For the Iberia trough index, a weaker (marginal significance) connection was found with EAWR, as well as with the Scandinavian mode (Barnston and Livezey, 1987). These findings warrant further investigation to understand the common variance, while exploring the added value of the trough indices.

## 7 | CONCLUSIONS

This study has shown that a systematic downstream response to upper-level wintertime troughs over Iberia and CMed is low-level warming over NE Africa that spreads southeast across North Africa and persists at low latitudes for a few days to over a week. February NEC strong MCS events were previously related to such a sequence (T18); this type of connection is now found (with schematic summary in Figure 11): (i) to be active throughout boreal winter months (November–March), (ii) to link with general rainfall and convective activity over a wider zone than NEC (including NWC and EGC), and (iii) to have wider synoptic weather expression as well across much of North Africa and surrounding region including southwestern Asia and eastern Africa. Some differences are noted depending on the several-day sequence of Iberia and CMed conditions (Figure 7), which needs to be factored in both for climate studies and weather forecasting.

Warming at such tropical latitudes does not occur following upper-level troughs over the Atlantic (nor troughs  $15^{\circ}$  east of CMed). This suggests a role for processes unique to the African continental setting. It is proposed that for troughs extending from Iberia to CMed, geography and climate dynamics deliver the opportunity to excite this sequence. Further diagnostic work is needed to more precisely assess the trough anchor longitudes that enable the downstream low latitude several-day warming, while the mechanisms exciting the warming response require process-oriented investigation. Further analyses should also seek to clarify the linkages between warming to the north of NC and key atmospheric variables associated with NC rainfall, especially given the

data sparsity in this region. Particular caution is attributed to reanalysis moisture, although its alignment here with OLR is encouraging. Overall, our results do support positive T850 anomalies north of NC leading key atmospheric developments and rainfall/convection over NC (Figure 11).

A secondary more minor route for troughs to influence NC emerges through direct teleconnection of troughs to equatorial SWA moisture and convection anomalies (Knippertz and Fink, 2008). Following Iberia troughs, once such SWA anomalies are established (here for the domains WGC and EGC), they are found to migrate eastward into NWC and NEC, which appears in part through internal dynamics (this multi-day tendency occurs despite individual MCSs tending to migrate east-to-west). However, warming is also occurring in west-to-east sequence to the north of the rainfall belt, so this is likely also a driving factor in the migration of convection (the sequence is depicted in Figure 11a). Finally, for some NC rainfall events, a direct link to remnants of a strong CMed trough through a southwest-northeast plume of moisture (Figure 11b) requires more explicit investigation. Indeed, many of the findings presented here will benefit from targeted atmospheric modelling and moisture/energy budget analyses to better reveal the underpinning mechanisms and build further confidence.

The NC—midlatitude linkages reported here are clearly distinct from linkages found with the main rainy seasons of the Congo Basin, where research has identified connections into the tropical Atlantic and northward to the NAO (e.g., Todd and Washington, 2004), or to implied changes in the Walker circulation (e.g., Camberlin *et al.*, 2001). In addition, it is noted that no obvious expression of the Madden–Julian Oscillation or similar equatorial modes is present in the leading NC composites, although it is possible that a contributing role will emerge in targeted research.

The overall synoptic sequence reported here is seen in seasonal teleconnection expression and represents a framework to interpret climate variation and change in the region (as in T18). Optimal seasonal indices combining daily trough activity from Iberia to CMed may draw on frequency, intensity, movement, and dynamics. Such indices may also be useful in statistical forecasting approaches, especially given the low skill in ensemble rainfall predictions in equatorial Africa (Vogel *et al.*, 2020). Nevertheless, the results here should already be valuable in increasing the situational awareness of operational weather forecasters across the impacted domain.

## ACKNOWLEDGEMENTS

The authors are grateful to the two reviewers whose comments helped substantially improve the manuscript. The

authors are grateful to the data providers: ERA5 provided by Copernicus Data Store through <https://www.ecmwf.int/en/forecasts/datasets/reanalysis-datasets/era5>, Interpolated OLR data provided by NOAA/OAR/ESRL PSL <https://psl.noaa.gov/>; IMERG provided by NASA <https://disc.gsfc.nasa.gov/>; Indices of teleconnection modes provided by NOAA/CPC <https://www.cpc.ncep.noaa.gov/data/teledoc/telecontents.shtml>. Marsham and Parker have been supported by AMMA-2050, IMPALA (NERC/DFID NE/M020126/1 and NE/M017176/1); Marsham, Parker and Taylor by UK Research and Innovation as part of the Global Challenges Research Fund, African SWIFT programme, grant number NE/P021077/1; Guichard has been supported by AMMA-2050 (NERC/DFID NE/M019950/1); Christopher M. Taylor by AMMA2050 (NE/M020428/2) and IMPALA (NE/M017230/1); and Richard J. Keane by CEMAC, University of Leeds. The second author acknowledges support from the Transregional Collaborative Research Center SFB/TRR 165 “Waves to Weather” ([www.wavestoweather.de](http://www.wavestoweather.de)) funded by the German Research Foundation (DFG).

## ORCID

Neil Ward  <https://orcid.org/0000-0003-1385-0349>

Andreas H. Fink  <https://orcid.org/0000-0002-5840-2120>

## REFERENCES

- Afifi, A. and Azen, S. (1979) *Statistical Analysis: A Computer Oriented Approach*, 2nd edition. New York: Academic Press.
- Alfaro, D.A. (2017) Low-tropospheric shear in the structure of squall lines: impacts on latent heating under layer-lifting ascent. *Journal of the Atmospheric Sciences*, 74(1), 229–248. <https://doi.org/10.1175/JAS-D-16-0168.1>.
- Balas, N., Nicholson, S. and Klotter, D. (2007) The relationship of rainfall variability in West Central Africa to sea-surface temperature fluctuations. *International Journal of Climatology: A Journal of the Royal Meteorological Society*, 27(10), 1335–1349. <https://doi.org/10.1002/joc.1456>.
- Barnston, A.G. and Livezey, R.E. (1987) Classification, seasonality and persistence of low-frequency atmospheric circulation patterns. *Monthly Weather Review*, 115(6), 1083–1126. [https://doi.org/10.1175/1520-0493\(1987\)115%3C1083:CSAPOL%3E2.0.CO;2](https://doi.org/10.1175/1520-0493(1987)115%3C1083:CSAPOL%3E2.0.CO;2).
- Bartlett, M. (1935) Some aspects of the time-correlation problem in regard to tests of significance. *Journal of the Royal Statistical Society*, 98(3), 536–543. <https://doi.org/10.2307/2342284>.
- Bekele-Biratu, E., Thiaw, W.M. and Korecha, D. (2018) Sub-seasonal variability of the Belg rains in Ethiopia. *International Journal of Climatology*, 38(7), 2940–2953. <https://doi.org/10.1002/joc.5474>.
- Bretherton, C.S., Widmann, M., Dymnikov, V.P., Wallace, J.M. and Bladé, I. (1999) The effective number of spatial degrees of freedom of a time-varying field. *Journal of Climate*, 12(7), 1990–2009. [https://doi.org/10.1175/1520-0442\(1999\)012%3C1990:TENOSD%3E2.0.CO;2](https://doi.org/10.1175/1520-0442(1999)012%3C1990:TENOSD%3E2.0.CO;2).

- Browning, K.A. and Ludlam, F. (1962) Airflow in convective storms. *Quarterly Journal of the Royal Meteorological Society*, 88(376), 117–135. <https://doi.org/10.1002/qj.49708837602>.
- Camberlin, P., Barraud, G., Bigot, S., Dewitte, O., Makanzu Imwangana, F., Maki Mateso, J.C., Martiny, N., Monsieurs, E., Moron, V., Pellarin, T., Philippon, N., Sahani, M. and Samba, G. (2019) Evaluation of remotely sensed rainfall products over Central Africa. *Quarterly Journal of the Royal Meteorological Society*, 145(722), 2115–2138. <https://doi.org/10.1002/qj.3547>.
- Camberlin, P., Janicot, S. and Pocard, I. (2001) Seasonality and atmospheric dynamics of the teleconnection between African rainfall and tropical sea-surface temperature: Atlantic vs. ENSO. *International Journal of Climatology: A Journal of the Royal Meteorological Society*, 21(8), 973–1005. <https://doi.org/10.1002/joc.673>.
- Camberlin, P. and Philippon, N. (2002) The east African march-may rainy season: associated atmospheric dynamics and predictability over the 1968–97 period. *Journal of Climate*, 15(9), 1002–1019. [https://doi.org/10.1175/1520-0442\(2002\)015%3C1002:TEAMMR%3E2.0.CO;2](https://doi.org/10.1175/1520-0442(2002)015%3C1002:TEAMMR%3E2.0.CO;2).
- Cook, K.H. (2000) The South Indian convergence zone and inter-annual rainfall variability over southern Africa. *Journal of Climate*, 13(21), 3789–3804. [https://doi.org/10.1175/1520-0442\(2000\)013%3C3789:TSICZA%3E2.0.CO;2](https://doi.org/10.1175/1520-0442(2000)013%3C3789:TSICZA%3E2.0.CO;2).
- Davis, J., Knippertz, P. and Fink, A.H. (2013) The predictability of precipitation episodes during the West African dry season. *Quarterly Journal of the Royal Meteorological Society*, 139(673), 1047–1058. <https://doi.org/10.1002/qj.2014>.
- Dee, D.P., Uppala, S.M., Simmons, A.J., Berrisford, P., Poli, P., Kobayashi, S., Andrae, U., Balmaseda, M.A., Balsamo, G., Bauer, P., Bechtold, P., Beljaars, A.C.M., van de Berg, L., Bidlot, J., Bormann, N., Delsol, C., Dragani, R., Fuentes, M., Geer, A.J., Haimberger, L., Healy, S.B., Hersbach, H., Hólm, E. V., Isaksen, L., Kållberg, P., Köhler, M., Matricardi, M., McNally, A.P., Monge-Sanz, B.M., Morcrette, J.J., Park, B.K., Peubey, C., de Rosnay, P., Tavolato, C., Thépaut, J.N. and Vitart, F. (2011) The ERA-interim reanalysis: configuration and performance of the data assimilation system. *Quarterly Journal of the Royal Meteorological Society*, 137(656), 553–597. <https://doi.org/10.1002/qj.828>.
- Dezfuli, A. (2017) Climate of western and central equatorial Africa. In: *Oxford Research Encyclopedia of Climate Science*. <https://doi.org/10.1093/acrefore/9780190228620.013.511>.
- Dezfuli, A.K. and Nicholson, S.E. (2013) The relationship of rainfall variability in western equatorial Africa to the tropical oceans and atmospheric circulation. Part II: the boreal autumn. *Journal of Climate*, 26(1), 66–84. <https://doi.org/10.1175/JCLI-D-11-00686.1>.
- Finney, D.L., Marsham, J.H., Walker, D.P., Birch, C.E., Woodhams, B.J., Jackson, L.S. and Hardy, S. (2020) The effect of westerlies on East African rainfall and the associated role of tropical cyclones and the Madden–Julian Oscillation. *Quarterly Journal of the Royal Meteorological Society*, 146(727), 647–664. <https://doi.org/10.1002/qj.3698>.
- Fröhlich, L., Knippertz, P., Fink, A.H. and Hohberger, E. (2013) An objective climatology of tropical plumes. *Journal of Climate*, 26(14), 5044–5060. <https://doi.org/10.1175/JCLI-D-12-00351.1>.
- Hart, N.C., Washington, R. and Maidment, R.I. (2019) Deep convection over Africa: annual cycle, ENSO, and trends in the hot-spots. *Journal of Climate*, 32(24), 8791–8811. <https://doi.org/10.1175/JCLI-D-19-0274.1>.
- Hersbach, H., Bell, B., Berrisford, P., Hirahara, S., Horányi, A., Muñoz-Sabater, J., Nicolas, J., Peubey, C., Radu, R., Schepers, D., Simmons, A., Soci, C., Abdalla, S., Abellan, X., Balsamo, G., Bechtold, P., Biavati, G., Bidlot, J., Bonavita, M., Chiara, G., Dahlgren, P., Dee, D., Diamantakis, M., Dragani, R., Flemming, J., Forbes, R., Fuentes, M., Geer, A., Haimberger, L., Healy, S., Hogan, R.J., Hólm, E., Janisková, M., Keeley, S., Laloyaux, P., Lopez, P., Lupu, C., Radnoti, G., Rosnay, P., Rozum, I., Vamborg, F., Villaume, S. and Thépaut, J.N. (2020) The ERA5 global reanalysis. *Quarterly Journal of the Royal Meteorological Society*, 146, 1999–2049. <https://doi.org/10.1002/qj.3803>.
- Hirst, A.C. and Hastenrath, S. (1983) Diagnostics of hydrometeorological anomalies in the Zaire (Congo) basin. *Quarterly Journal of the Royal Meteorological Society*, 109(462), 881–892. <https://doi.org/10.1002/qj.49710946213>.
- Hua, W., Zhou, L., Chen, H., Nicholson, S.E., Jiang, Y. and Raghavendra, A. (2018) Understanding the Central Equatorial African long-term drought using AMIP-type simulations. *Climate Dynamics*, 50(3–4), 1115–1128. <https://doi.org/10.1007/s00382-017-3665-2>.
- Huffman, G.J., Stocker, E.F., Bolvin, D.T., Nelkin, E.J. and Tan, J. (2019) In: Savtchenko, A. and Greenbelt, M.D. (Eds.) *GPM IMERG Final Precipitation L3 1 Day 0.1 Degree x 0.1 Degree V06*. Greenbelt, Maryland: Goddard Earth Sciences Data and Information Services Center (GES DISC). <https://doi.org/10.5067/GPM/IMERGDF/DAY/06>.
- Ionita, M. (2014) The impact of the East Atlantic/Western Russia pattern on the hydroclimatology of Europe from mid-winter to late spring. *Climate*, 2(4), 296–309. <https://doi.org/10.3390/cli2040296>.
- Jackson, B., Nicholson, S.E. and Klotter, D. (2009) Mesoscale convective systems over western equatorial Africa and their relationship to large-scale circulation. *Monthly Weather Review*, 137(4), 1272–1294. <https://doi.org/10.1175/2008MWR2525.1>.
- Jackson, L.S., Keane, R.J., Finney, D.L., Marsham, J.H., Parker, D. J., Senior, C.A. and Stratton, R.A. (2019) Regional differences in the response of rainfall to convectively coupled kelvin waves over tropical Africa. *Journal of Climate*, 32(23), 8143–8165. <https://doi.org/10.1175/JCLI-D-19-0014.1>.
- Jacobeit, J. (1987) Variations of trough positions and precipitation patterns in the Mediterranean area. *Journal of Climatology*, 7(5), 453–476. <https://doi.org/10.1002/joc.3370070503>.
- Klein, C. and Taylor, C.M. (2020) Dry soils can intensify mesoscale convective systems. *Proceedings of the National Academy of Sciences*, 117(35), 21132–21137. <https://doi.org/10.1073/pnas.2007998117>.
- Knippertz, P. (2004) A simple identification scheme for upper-level troughs and its application to winter precipitation variability in Northwest Africa. *Journal of Climate*, 17(6), 1411–1418. [https://doi.org/10.1175/1520-0442\(2004\)017%3C1411:ASISFU%3E2.0.CO;2](https://doi.org/10.1175/1520-0442(2004)017%3C1411:ASISFU%3E2.0.CO;2).
- Knippertz, P. (2007) Tropical–extratropical interactions related to upper-level troughs at low latitudes. *Dynamics of Atmospheres*

- and Oceans, 43(1–2), 36–62. <https://doi.org/10.1016/j.dynatmoce.2006.06.003>.
- Knippertz, P. and Fink, A.H. (2008) Dry-season precipitation in tropical West Africa and its relation to forcing from the extratropics. *Monthly Weather Review*, 136(9), 3579–3596. <https://doi.org/10.1175/2008MWR2295.1>.
- Knippertz, P. and Fink, A.H. (2009) Prediction of dry-season precipitation in tropical West Africa and its relation to forcing from the extratropics. *Weather and Forecasting*, 24(4), 1064–1084. <https://doi.org/10.1175/2009WAF2222221.1>.
- Laing, A.G., Carbone, R.E. and Levizzani, V. (2011) Cycles and propagation of deep convection over equatorial Africa. *Monthly Weather Review*, 139(9), 2832–2853. <https://doi.org/10.1175/2011MWR3500.1>.
- Lavaysse, C., Flamant, C., Janicot, S., Parker, D., Lafore, J.-P., Sultan, B. and Pelon, J. (2009) Seasonal evolution of the West African heat low: a climatological perspective. *Climate Dynamics*, 33(2–3), 313–330. <https://doi.org/10.1007/s00382-009-0553-4>.
- Lazenby, M.J., Todd, M.C. and Wang, Y. (2016) Climate model simulation of the South Indian Ocean convergence zone: mean state and variability. *Climate Research*, 68(1), 59–71. <https://doi.org/10.3354/cr01382>.
- Liebmann, B. and Smith, C.A. (1996) Description of a complete (interpolated) outgoing longwave radiation dataset. *Bulletin of the American Meteorological Society*, 77(6), 1275–1277. <https://www.jstor.org/stable/26233278>.
- Maranan, M., Fink, A.H. and Knippertz, P. (2018) Rainfall types over southern West Africa: Objective identification, climatology and synoptic environment. *Quarterly Journal of the Royal Meteorological Society*, 144(714), 1628–1648. <https://doi.org/10.1002/qj.3345>.
- Matthews, A.J. (2012) A multiscale framework for the origin and variability of the South Pacific Convergence Zone. *Quarterly Journal of the Royal Meteorological Society*, 138(666), 1165–1178. <https://doi.org/10.1002/qj.1870>.
- Nicholson, S.E. (1981) Rainfall and atmospheric circulation during drought periods and wetter years in West Africa. *Monthly Weather Review*, 109(10), 2191–2208. [https://doi.org/10.1175/1520-0493\(1981\)109%3C2191:RAACDD%3E2.0.CO;2](https://doi.org/10.1175/1520-0493(1981)109%3C2191:RAACDD%3E2.0.CO;2).
- Nicholson, S.E. and Dezfuli, A.K. (2013) The relationship of rainfall variability in western equatorial Africa to the tropical oceans and atmospheric circulation. Part I: the boreal spring. *Journal of Climate*, 26(1), 45–65. <https://doi.org/10.1175/JCLI-D-11-00653.1>.
- Rotunno, R., Klemp, J.B. and Weisman, M.L. (1988) A theory for strong, long-lived squall lines. *Journal of the Atmospheric Sciences*, 45(3), 463–485. [https://doi.org/10.1175/1520-0469\(1988\)045%3C0463:ATFSSL%3E2.0.CO;2](https://doi.org/10.1175/1520-0469(1988)045%3C0463:ATFSSL%3E2.0.CO;2).
- Salerno, J., Diem, J.E., Konecky, B.L. and Hartter, J. (2019) Recent intensification of the seasonal rainfall cycle in equatorial Africa revealed by farmer perceptions, satellite-based estimates, and ground-based station measurements. *Climatic Change*, 153(1–2), 123–139. <https://doi.org/10.1007/s10584-019-02370-4>.
- Samba, G. and Nganga, D. (2012) Rainfall variability in Congo-Brazzaville: 1932–2007. *International Journal of Climatology*, 32(6), 854–873. <https://doi.org/10.1002/joc.2311>.
- Skinner, C.B. and Poulsen, C.J. (2016) The role of fall season tropical plumes in enhancing Saharan rainfall during the African Humid Period. *Geophysical Research Letters*, 43(1), 349–358. <https://doi.org/10.1002/2015GL066318>.
- Taylor, C.M., Fink, A.H., Klein, C., Parker, D.J., Guichard, F., Harris, P.P. and Knapp, K.R. (2018) Earlier seasonal onset of intense mesoscale convective systems in The Congo Basin since 1999. *Geophysical Research Letters*, 45(24), 13,458–13,467. <https://doi.org/10.1029/2018GL080516>.
- Todd, M.C. and Washington, R. (2004) Climate variability in central equatorial Africa: influence from the Atlantic sector. *Geophysical Research Letters*, 31(31), L23202. <https://doi.org/10.1029/2004GL020975>.
- Van Der Wiel, K., Matthews, A.J., Stevens, D.P. and Joshi, M.M. (2015) A dynamical framework for the origin of the diagonal South Pacific and South Atlantic convergence zones. *Quarterly Journal of the Royal Meteorological Society*, 141(691), 1997–2010. <https://doi.org/10.1002/qj.2508>.
- Vizy, E.K. and Cook, K.H. (2014) Impact of cold air surges on rainfall variability in the Sahel and wet African tropics: a multi-scale analysis. *Climate Dynamics*, 43(3–4), 1057–1081. <https://doi.org/10.1007/s00382-013-1953-z>.
- Vogel, P., Knippertz, P., Fink, A.H., Schlueter, A. and Gneiting, T. (2020) Skill of global raw and postprocessed ensemble predictions of rainfall in the tropics. *Weather and Forecasting*, 35, 2367–2385. <https://doi.org/10.1175/WAF-D-20-0082.1>.
- Washington, R., James, R., Pearce, H., Pokam, W.M. and Moufouma-Okia, W. (2013) Congo Basin rainfall climatology: can we believe the climate models? *Philosophical Transactions of the Royal Society B: Biological Sciences*, 368(1625), 20120296. <https://doi.org/10.1098/rstb.2012.0296>.
- Wilkie, D., Morelli, G., Rotberg, F. and Shaw, E. (1999) Wetter isn't better: global warming and food security in the Congo Basin. *Global Environmental Change*, 9(4), 323–328. [https://doi.org/10.1016/S0959-3780\(99\)00021-7](https://doi.org/10.1016/S0959-3780(99)00021-7).

## SUPPORTING INFORMATION

Additional supporting information may be found online in the Supporting Information section at the end of this article.

**How to cite this article:** Ward N, Fink AH, Keane RJ, *et al.* Synoptic timescale linkage between midlatitude winter troughs Sahara temperature patterns and northern Congo rainfall: A building block of regional climate variability. *Int J Climatol.* 2021;41:3153–3173. <https://doi.org/10.1002/joc.7011>